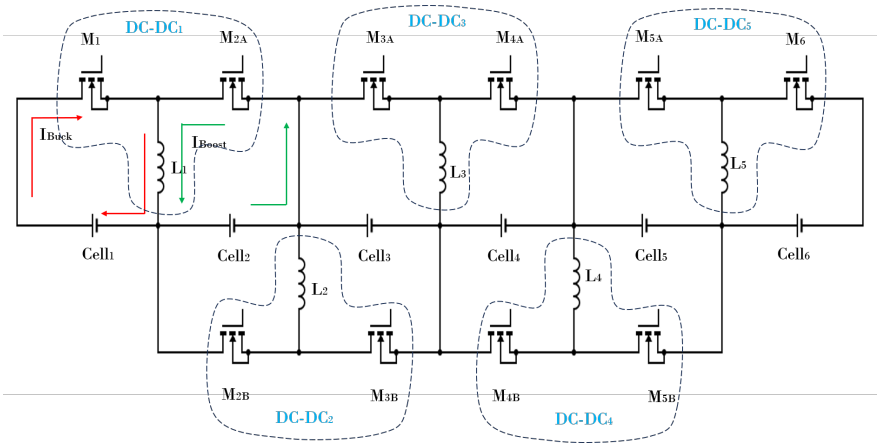

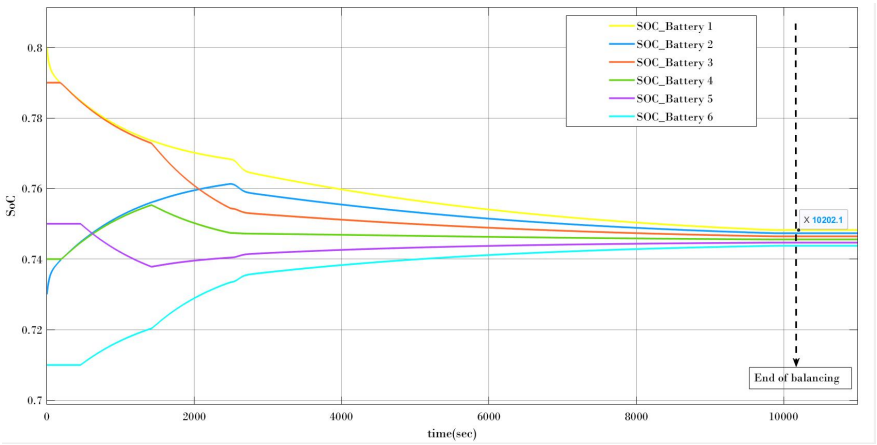

Modelling and Simulation of DC/DC Converter-Based Active Cell Balancing for Battery Management Systems

Master's thesis in Electrical Engineering

VIKAS GANAGAMAGALA MAHANTHAPPA
SRINIDHI SOLLAPURA VASANNA
DEPARTMENT OF ELECTRICAL ENGINEERING
CHALMERS UNIVERSITY OF TECHNOLOGY
Gothenburg, Sweden 2024
www.chalmers.se

Master's thesis 2024

Modelling and Simulation of DC/DC Converter-Based Active Cell Balancing for Battery Management Systems

VIKAS GANGAMAGALA MAHANTHAPPA
SRINIDHI SOLLAPURA VASANNA

CHALMERS
UNIVERSITY OF TECHNOLOGY

Department of Electrical Engineering
Chalmers University of Technology
Gothenburg, Sweden 2024

Modelling and Simulation of DC/DC Converter-Based Active Cell Balancing for Battery Management Systems

Vikas Gangamagala Mahanthappa
Srinidhi Sollapura Vasanna

© Vikas Gangamagala Mahanthappa, Srinidhi Sollapura Vasanna 2024.

Supervisor: Yang Li, Researcher at Automatic Control, Department of Electrical Engineering
Examiner: Changfu Zou, Associate Professor at Automatic Control, Department of Electrical Engineering

Master's Thesis 2024
Department of Electrical Engineering
Chalmers University of Technology
SE-412 96 Gothenburg
Telephone +46 31 772 1000

Cover: Battery Modelling of the Electro-chemical model to Electrical circuit model, showing the internal resistance and open circuit voltage depicting the chemical reaction inside the battery for the flow of electrons and ions.

Typeset in LaTeX
Printed by Chalmers Reproservice
Gothenburg, Sweden 2024

Modelling and Simulation of DC/DC Converter-Based Active Cell Balancing for Battery Management Systems
Vikas Gangamagala Mahanthappa
Srinidhi Sollapura Vasanna
Department of Electrical Engineering
Chalmers University of Technology

Abstract

The transition to sustainable transportation was initiated to mitigate the effects of global warming and decrease CO_2 emissions. Electric vehicles are at the forefront of this revolution and rapid technological advancements have been made in the development of electric powertrain's components, particularly lithium-ion (Li-ion) batteries. These breakthroughs have played a significant role in increasing vehicle performance and range, prompting automotive companies to accelerate their transition to more sustainable vehicles. Li-ion batteries are prominent in their specific energy and specific power while the battery pack comprises low-voltage battery cells connected in series and parallel to meet the voltage and current requirements of the electric vehicles. However, since the cells are limited by voltage and capacity, a serious inconsistency between the cell's voltage and state of charge (SoC) is generated because of the manufacturing inconsistencies of the individual cells in the battery pack. This leads to growth over time after a number of charging and discharging cycles because of different self-discharge rates, internal resistance, and operating temperature, which will affect the efficiency and life of the entire battery pack. It has become inevitable to keep the cells balanced to achieve the effective usage of energy and to enhance the battery life.

This thesis starts with a comprehensive literature study and investigation of different types of cell balancing techniques with a focus on converter-based active balancing. A choice has been made after evaluating the performance and suitability of different converters considering the balancing method, balancing speed, balancing time, and control complexity. In MATLAB/Simulink, a bi-directional buck-boost converter was designed and simulated by integrating with the battery string, performing energy exchange between cells with different SoCs using a state-space modeling approach and cascaded PID control. An easy-to-implement and effective algorithm has been developed, tested, and validated to perform the balancing action in various operating scenarios.

Keywords: Li-ion battery, Active cell balancing, Converter based active balancing, Bidirectional Buck-boost converter, Battery management system, Energy management system, Electric vehicle.

Acknowledgements

The thesis work has been carried out at the Department of Electrical Engineering at Chalmers University of Technology, Gothenburg, Sweden, and Knightec AB, Gothenburg, Sweden.

We would like to express our deepest gratitude and appreciation to our supervisor Yang Li for his constant support, guidance, and engagement, who has been a backbone for us in this journey, and examiner Changfu Zou, for always being empathetic and supportive.

We would also like to extend our heartfelt thanks to the faculty members of Knightec AB, namely Ola Löfquist, Rohit Puthukode Ramakrishnan, and Rahul Puthukode Ramakrishnan, for their valuable input, feedback, and encouragement. Also, Fredrik Björndahl, thank him for giving us this opportunity to work on this interesting subject. Their expertise and enthusiasm have been inspiring, and their commitment to excellence has shaped our academic pursuits.

We would like to express our appreciation and gratitude to our friends: Varun Ramakrishnan Bharadwaj, Nitesh Anil Kumar Nikkam, Navaneet Subbaram, Bhanushree Munegowda, Olle Johnson, and Umberto Frateily for their helping hands with this thesis who have contributed to the creation of this thesis, whether through their comments, suggestions, or encouragement. Their feedback and support have been invaluable in shaping our ideas, refining our arguments, and improving our writing skills.

Completing this thesis has been a challenging yet rewarding journey and would not have been possible without the contributions and support of all those mentioned above. Their collective efforts have played an integral role in the successful completion of this research endeavor. We are humbled and grateful for their invaluable contributions.

Vikas Gangamagala Mahanthappa, Gothenburg, 2024
Srinidhi Sollapura Vasanna, Gothenburg, 2024

List of Acronyms

Below is the list of acronyms that have been used throughout this thesis listed in alphabetical order:

V	Voltage
I	Current
T	Temperature
EV	Electric Vehicle
BMS	Battery Management System
SoC	State of Charge
SoH	State of Health
DoD	Depth of Discharge
R_i	Internal Resistance
CE	Coulomb Efficiency
ACTC	Adjacent Cell-to-Cell
DCTC	Direct Cell-to-Cell
CTP	Cell-to-Pack
PTC	Pack-to-Cell
CTPTC	Cell-to-Pack-to-Cell
PDAE	Partial Differential-Algebraic Equations
LPM	Lumped-Parameter Models
DAE	Differential Algebraic Equation
RC	Resistance-Capacitance
OCV	Open-Circuit Voltage
KF	Kalman Filter
EKF	Extended Kalman Filter
AEKF	Adaptive Extended Kalman Filter
UKF	Unscented Kalman Filter
FL	Fuzzy Logic
HVAC	Heating, Ventilation, and Air Conditioning
ELAC	Electrical Air Compressor
PWM	Pulse Width Modulation
ECU	Electronic Control Unit
MCU	Main Control Unit
HV	High Voltage
LV	Low Voltage
CAN	Controller Area Network

LIN	Local Interconnect Network
BDU	Battery Disconnect Unit
DTC	Diagnostic Trouble Code
DID	Data Identifier Code
HMI	Human Machine Interface
LED	Light-Emitting Diode
PID	Proportional, Integral, Derivative

Contents

List of Figures

List of Tables

1
Introduction

The evolution of mobility is increasingly focused on sustainable transportation to address the urgent need for mitigating the effects of global warming and reducing CO_2 emissions. Substantial research and development are being invested to promote electric vehicles (EVs) equipped with new energy storage technologies. The implementation of rechargeable batteries in EVs has become indispensable. Different types of battery energy storage, such as nickel-metal hydride (NiMH), lead acid, and lithium-ion (Li-ion) batteries, have been tested and deployed, and are currently dominating the market. The Li-ion battery, in particular, has gained widespread acceptance due to its high energy density, high efficiency, and long lifespan when compared to the rest [1]. The most commonly used types of Li-ion batteries in modern applications include lithium cobalt oxide ($LiCoO_2$ or LCO), lithium manganese oxide ($LiMn_2O_4$), lithium iron phosphate ($LiFePO_4$ or LFP), lithium nickel–manganese-cobalt oxide ($LiNiMnCoO_2$ or NMC), lithium nickel cobalt aluminum oxide ($LiNiCoAlO_2$ or NCA) and lithium titanate ($Li4Ti_5O_{12}$ or LTO) [2].

1.1 Problem Background

A single Li-ion cell can only typically provide a nominal voltage of around 3.6–3.8 V, and a number of cells have to be connected in series and in parallel to serve the overall energy and power requirements of the vehicle. Inter-cell inconsistency is becoming an inevitable problem that increases with the number of cells in the battery pack, which worsens with the repeated charge/discharge cycle [3].

The causes of the inconsistency can be divided into two categories: Internal inconsistency factors and external inconsistency factors. Internal factors arise from cell manufacturing and assembly flaws, causing variations in initial conditions such as internal resistance, capacity, coulombic efficiency, state of charge (SoC), and self-discharge rate [4, 5]. Such inconsistency is inevitable, constituting the initial imbalance throughout the battery pack. On the other hand, factors like different operating conditions during charging and discharging and the different cell localization in a battery pack lead to operating at different temperatures and SoC [6, 7].

The significant impact of this inconsistency leads to undesired consequences. Exceeding voltage thresholds can lead to certain cells becoming overcharged or over-discharged. Overcharging a cell may cause an explosion and fire while over-discharging a cell accelerates the aging of the battery and reduces charge capacity [8].

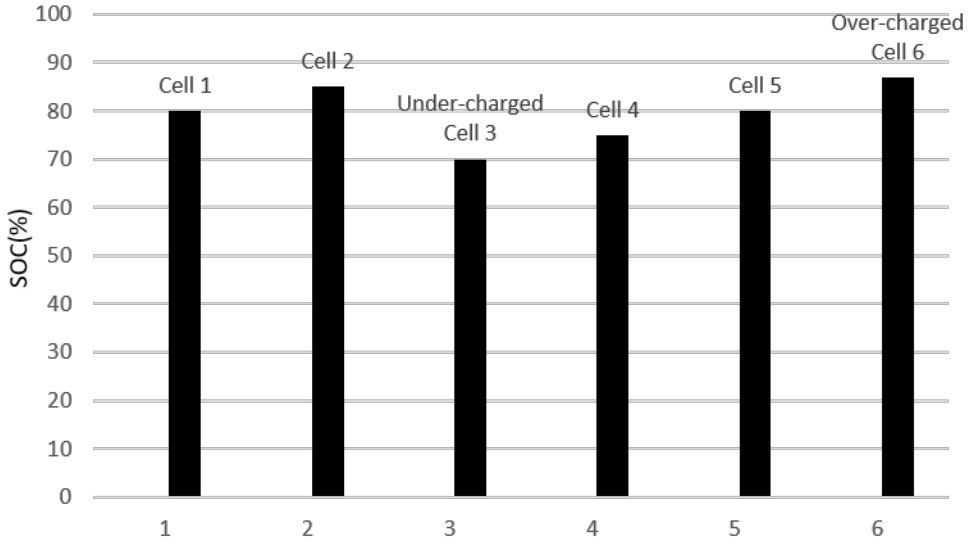

Figure 1.1: Unbalanced cells in terms of SoC. 80% is considered the charging target here.

In addition, the battery pack's charge level is determined by the cell with the lowest charge capacity among the cells connected in series. If the safe operating voltage limit is exceeded, the charging or discharging process is forced to stop in order to protect the battery from safety hazards. This premature charge termination reduces usable capacity significantly, affecting the battery pack's overall service performance [8]. Thus, as shown in Figure 1.1, the weakest cell in the battery pack will be the limiting cell during the charging or discharging process. If not well managed, the inconsistency of the cells will increase, yielding ineffective energy utilization in the battery pack.

To mitigate these problems, the cells must be monitored and controlled to operate at favorable conditions, which is usually handled by a battery management system (BMS), commonly termed a cell balancing or equalization system. A robust BMS is required to ensure the Li-ion batteries can run safely and reliably, prevent physical damage, and address temperature variations and cell unbalance [9]. Furthermore, different battery states, such as SoC and state of health (SoH), can be estimated in the BMS based on measured temperature, voltage, and current. The safety is guaranteed by alarms to prevent overcharging/over-discharging [10, 11]. The cell balancing unit serves to monitor the cell dynamic parameters and control the energy for effective utilization, contributing to the longevity of the battery pack.

Depending on the charge transfer mechanisms, there are two main types of cell balancing methods that may be adopted: Active balancing and passive balancing. The energy from all the cells is dissipated through the resistors in the passive balancing process before all the cells' SoCs reach the lowest SoC in the cells. This approach offers a straightforward circuit that is inexpensive and requires minimal maintenance.

The disadvantage of this approach is that besides the low efficiency due to the high energy loss, a lot of heat is generated inside the circuit, which requires additional effort for thermal management [12].

The idea of active balancing is to use an extra balancing circuit to shift energy from a high-SoC cell to a low-SoC cell. Active balancing is mainly classified as capacitor-based, transformer-based, and DC-DC converter-based while the topology is dependent on the energy transfer methods used during balancing. Generally, the energy can be transferred in different energy flow modes such as adjacent cell-to-cell (ACTC), direct cell-to-cell (DCTC), cell-to-pack (CTP), pack-to-cell (PTC), and cell-to-pack-to-cell (CTPTC) through the energy storage devices like a capacitor, transformer or using DC-DC converters. Active cell balancing achieves better efficiency and higher control performance than passive balancing methods, making it promising in automotive applications [13]. Choosing the balancing circuit depends on the requirements of the balancing efficiency, balancing time, control robustness, cost and size, etc.

1.2 Thesis Objective

The objective of this thesis work is to investigate different types of converter-based active balancing and implement the most suitable technique for achieving a highly-efficient Li-ion battery pack. A choice of converter should be made considering the performance and suitability of different designs. The system-level model will be built with Simulink to predict the dynamic behavior of the battery pack and the chosen converter for the design of the balancing algorithm as well as the feedback control system. The built model is operated at different unbalanced scenarios using different balancing algorithms to evaluate the performance of the proposed algorithm.

1.3 Limitations

This thesis work mainly focuses on developing the control algorithm and its implementation in the simulation software, emphasizing the importance and robustness of the DC-DC converter-based active balancing. A simple battery model consisting of a DC voltage source connected in series with a resistor is considered to depict the basic characteristics of the battery including terminal voltage, current, power, overpotential, and SoC, where other parameters such as SoH, battery aging, and thermal behavior were not considered and studied. Furthermore, the balancing model scaled down to handle only six cells connected in series for the purposes of demonstration, and more complex configurations with parallel units are not focused.

2
Theory

This chapter presents an overview of vehicle schematics, BMS architecture, and cell balancing methods. Section 2.1 presents the vehicle schematics of different systems involved in an EV, Section 2.2 gives an introduction to BMS architecture, and Section 2.3 presents the battery characteristics during charging and discharging. Section 2.4 covers a comprehensive overview of cell balancing methods. Section 2.5 discusses the classification of active cell balancing. Section 2.6 introduces battery modeling techniques and the different types of battery models with their capability of capturing battery dynamics. Sections 2.7 and 2.8 are about SoC estimation and the controllers, respectively.

2.1 Vehicle Schematics

In a commercial vehicle, typical components include chassis, engine, transmission, fuel system, electrical system, suspension system, steering system, heating, ventilation, and air conditioning (HVAC) system, electrical air compressor (ELAC) system, body and interior and so on. Each system has critical, complex, and highly logical components that require an electronic control unit (ECU) to monitor, control, diagnose, communicate, and signal map between the two systems. All ECUs are signal-mapped in a way that they communicate with the main control unit (MCU) in an electrical architecture. A typical BMS operates under the high-voltage (HV) electronics system which involves interaction between the HV battery, DC/DC converter, HV-charging portals, and other small consumer loads [14].

Figure 2.1 shows an overview of the typical electrical system in an electric vehicle. It is described that the MCU works or serves as a central hub where it receives data from various ECUs and sensors in a vehicle's electrical architecture, through signal mapping between the ECUs. By processing data, the MCU controls the overall vehicle operation. All the above signal mapping and communication are made through different interfaces such as controller area network (CAN), local interconnect network (LIN), Ethernet or wireless (Wi-Fi or Bluetooth), etc [14, 15].

The battery disconnect unit (BDU) main functions to cut off the contactors (open-loop) or connect (closed-loop) the circuit of an HV line in the vehicle integrated system. To wake up or kick start the ECUs, one or more low-voltage (LV) batteries are utilized. Considering the above configuration on a vehicle level in the HV electronics system, high voltage to low voltage is converted where power is delivered to

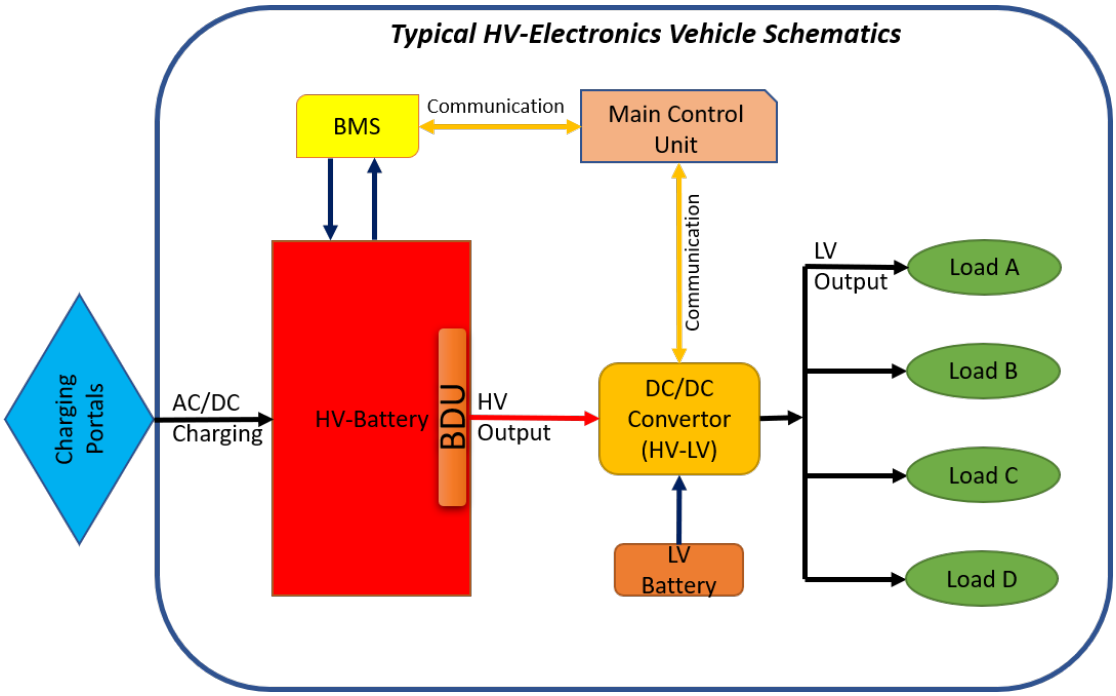

Figure 2.1: An overview of vehicle architecture for electrical systems.

different loads or consumers using the converter module [14, 15, 16]. The selection of this converter module is explained later.

2.2 BMS Architecture

Based on the critical functional aspect of an operating BMS, implementation criteria, application, and battery technology, BMS architecture consists of numerous components and subsystems to monitor and control the performance of a vehicle for better outcomes. A typical BMS architecture is shown in Figure 2.2. The subsystems in Figure 2.2 will be discussed in detail in the following sections.

2.2.1 Sensing, Measuring, and Monitoring

The BMS continually monitors the voltage (V), current (I), and temperature (T) of battery cells utilizing specific cell monitoring circuitry/sensors. Parameters such as the overall or individual cell voltage or current are measured using corresponding sensors, while non-measurable parameters (SoC, SoH, depth of discharge (DoD)) are calculated or monitored using algorithms such as Coulomb counting and state observers. Sensor data serve as input variables for the BMS to conduct its primary duties [3, 17].

2.2.2 Control

Control is a vital element that governs operation based on observed data from the vehicle system for guaranteed vehicle performance. For example, the temperature

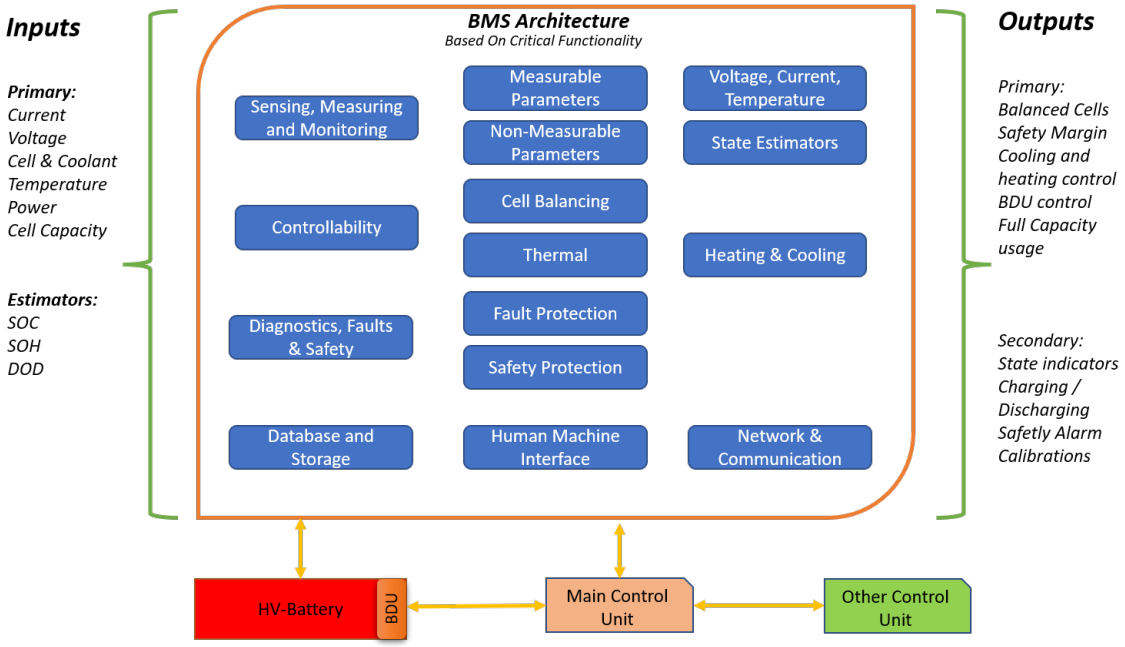

Figure 2.2: An overview of BMS architecture in an EV.

within the car is controlled by HVAC systems. Cell balancing increases battery life by increasing the utilization of the capacity of a battery pack. Furthermore, various control strategies avoid overcharging and undercharging during battery charging [17].

2.2.3 Diagnostics

Diagnostics are the capacity to identify or track any technical issue. It immediately raises alarms and warns the BMS in specific situations when the expected performance is not met. These include recognizing problems that respond with an error code, namely the diagnostic trouble code (DTC) that offers root cause information, and executing the diagnostic utilizing data identifier codes (DIDs) to check the system. Faults are often malfunctioning behaviors that cause system breakdowns and reduced performance. These can be electrical faults, mechanical faults, or software errors. Safety protocols are essential in a BMS because they reduce risks by preventing unintended human injury. For example, as described in the problem statement, owing to the irregularity in the SoC level, there might be an overcharge or overdischarge problem due to exceeding the voltage/current threshold in the cell, which could result in a fire or, in the worst-case scenario, an explosion. We need safety measures in the BMS to prevent these severe issues and safeguard the battery from dangerous occurrences. Protections are targeted to, short circuits, cyber-security, etc [18].

2.2.4 Database and Storage

A database is a digital or computerized storage space. In simple words, "A database is an environment where data is stored". It enables users to maintain, compute, manipulate, structure, and retrieve the data that could be used for future analysis [19].

2.2.5 Human Machine Interface (HMI)

To facilitate the interaction between the system and humans, an HMI is utilized. It serves as a bridge between the user and the machine, system, or device [20]. The HMI provides visual data interpretation of various subsystems in a BMS. For example, an HMI can display temperature, pressure, and other critical information for HVAC, as well as SoC information for battery usage. There are light-emitting diode indicators for additional alarm occurrences to assist in protecting the battery from harmful incidents [21].

2.2.6 Networking and Communication

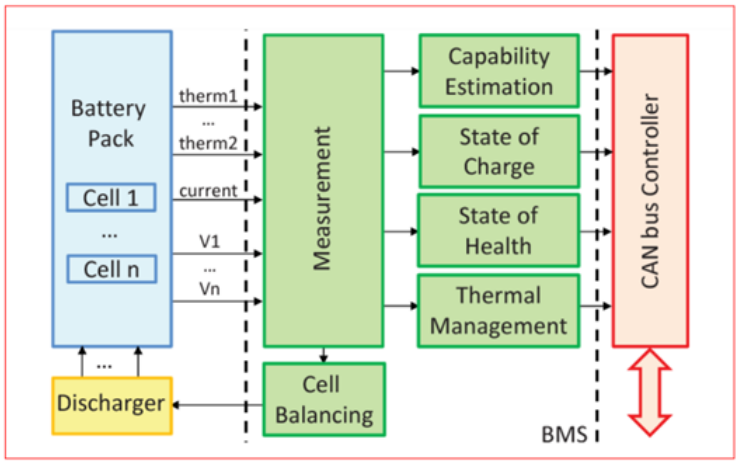

Figure 2.3: An overview of BMS communication in an EV [22].

In the BMS, industrial protocols such as CAN, LIN, Ethernet, or wireless communication are used to provide connections within the system or with an external device, where the data flow of measured values is continuously monitored to avoid risking factors such as the failure due to high or low temperature (thermal management), exceeding a high voltage or current threshold, low battery SoC level, among others [22]. Figure 2.3 shows an overview of the communication and the subsystem connections.

2.3 Battery Specifications

Battery exhibits nonlinear characteristics such as the SoC versus open-circuit voltage (OCV) relation. A typical relationship between SoC and OCV of an NMC cell is

shown in Figures 2.4 and 2.5 at different C-rates and temperatures, respectively [23].

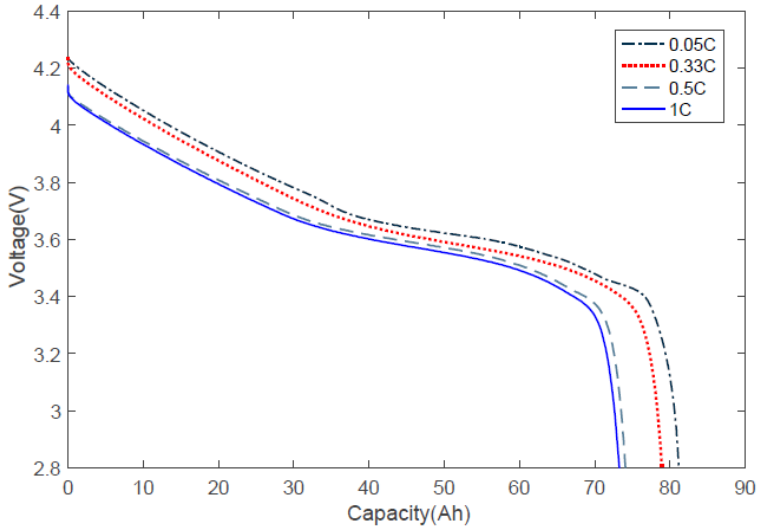

Figure 2.4: The discharge voltage curve at different C-rates as a function of battery capacity [23].

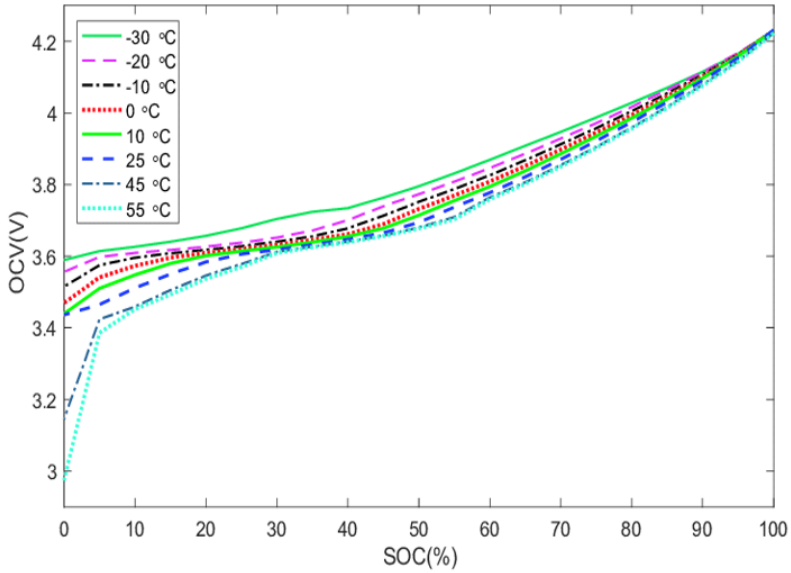

Figure 2.5: SOC-OCV relationship at different temperatures [23].

The technical specifications of any battery include parameters like nominal voltage, nominal capacity, operating voltage range, maximum C-rate, etc., which are given in Table 2.1. These parameters are very important in the study of the balancing process and controlling of the SoC.

2.4 An Overview of Cell Balancing

Cell balancing methods are broadly divided into passive and active balancing, where the excessive energy is wasted in the form of heat in passive balancing and the ex-

Table 2.1: Specifications for the typical industrial Li-ion cell [24].

Property	Value
Cell type	Li-ion
Cell nominal capacity	3.6 Ah
Cell nominal voltage	3.3 V
Cell operating voltage range	3.6 – 4.2 V
C-rate (max)	2.5C
Cathode material	NCA ($(LiNiCoAlO_2)$
Anode material	Graphite

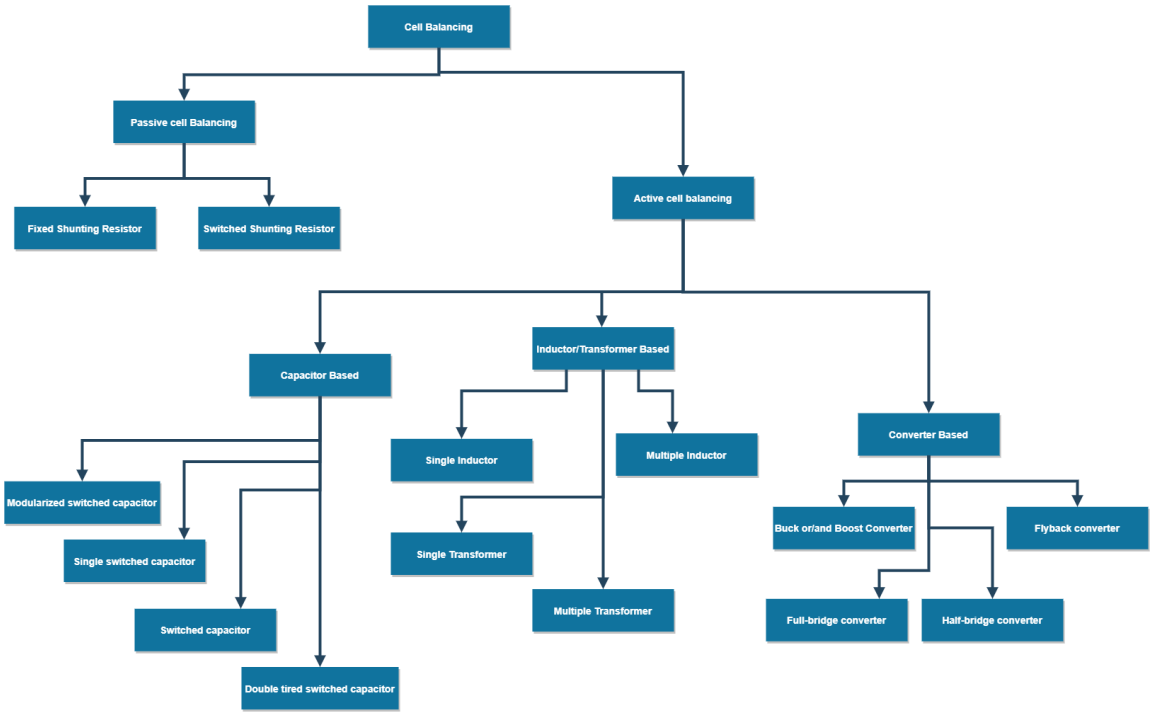

Figure 2.6: An overview of different cell balancing topologies.

cessive energy is transferred to different cells or to the weaker cells to balance the energy among all the cells.

Active cell balancing uses energy storage components, such as capacitors, transformers, inductors, and converters, to discharge the energy from the high SoC cells and redistributes it to the lower SoC cells. Compared to passive balancing, the energy losses in the form of heat are less, which facilitates highly efficient energy transfer [25].

Active cell balancing is mainly classified as that shown in Figure 2.6 and is further discussed in detail next.

2.4.1 Capacitor-Based Topology

In capacitor-based topology, the capacitors are considered to be the energy storage components that transfer the energy between the cells, and this is basically called 'charge shuttling' equalization. There are different configurations, such as those based on switched capacitors, double-tiered switched capacitors, single-switched capacitors, and modularized switched capacitors [26].

Switched capacitor balancing does not need intellectual control for the balancing process. However, it possesses a long equalization time and more expensive components like switches compared to passive balancing methods. Double-tiered capacitor balancing exhibits higher balancing speed, and the balancing time can be shortened by more than half. Single-switched capacitor balancing is a derivation of the switched capacitor method and it uses only one, but relatively bigger capacitor. Modularized switched capacitor balancing has been developed to balance the cells between the modules and the adjacent cells using the additional capacitors, but it yields a high cost [26].

Note that when the cell-to-cell dispersion is low, the balancing time can be long, and this is a crucial issue for all capacitor-based cell balancing methods [27].

2.4.2 Inductor/Transformer-Based Topology

Inductor/transformer-based topology uses an inductor/transformer to store the energy in the form of a magnetic field to transfer the charges from a higher voltage cell to a lower voltage cell.

Multi-inductor balancing uses multiple inductors to balance the cells simultaneously, but the disadvantage of this method is that only adjacent cells can be balanced directly. In the scenario that the cells at the extreme ends are in an imbalanced state, the charge has to be transferred from one end to another through the energy transfer into the cells in between, which yields a longer balancing time and also contributes to the loss of energy due to the multiple times of energy conversion [28].

Single-winding transformer balancing topology uses one transformer to transfer the energy between the cells through the cell-to-pack method or pack-to-cell method.

Multi-windings transformer balancing topology has a single magnetic core with one primary winding and multi secondary windings one for each cell, which requires n number of secondary windings for equalizing the n number of cells charge levels. It mainly includes *flyback topology* and *forward topology*, both offering better balancing performance compared to the single-winding transformer-based topology [29].

Compared to capacitor-based topologies, the inductor/transformer-based topology provides faster balancing speed but is hindered by the high cost, especially for the transformers. Also, to filter the high-frequency switching signals, filter capacitors need to be placed across each cell, which again adds extra cost and complexity for

the overall circuit [30].

2.4.3 DC-DC Converter-Based Topology

DC-DC converter-based active balancing uses the power electronics interface, to transfer the energy between different cells, with different modes of operation and the energy flow. This is achieved by using a bidirectional DC-DC converter that can both step up and step down the voltage of the cells. It has a significantly high balancing efficiency, robust design, high balancing speed, and high control degrees of freedom [29].

However, some challenges are also associated with DC-DC converter-based active cell balancing. One challenge is that the design of the balancing algorithm must balance the cells while taking into account the current and temperature of the cells. Another challenge is the cost of the DC-DC converter, which can be higher than that of other balancing designs [31].

2.5 Classification of Converter-Based Active Balancing

2.5.1 Based on Energy Flow

DC-DC converter-based active cell balancing can be classified into two sub-types based on the direction of energy flow: Unidirectional and bidirectional.

- *Unidirectional balancing* involves the transfer of energy from one or more high-voltage cells to one or more low-voltage cells. This type of balancing is used in applications where the battery pack has a fixed voltage range and the energy can only flow in one direction. Unidirectional balancing can be implemented using either step-up or step-down DC-DC converters [32].

- *Bidirectional balancing* involves the transfer of energy in both directions between cells. This type of balancing is used in applications where the battery pack has a variable voltage range and the energy needs to flow in both directions. Bidirectional balancing can be implemented using a bidirectional DC-DC converter [33].

Also, from the perspective of cell charge transfer, cell balancing can be performed using different energy flow topologies, each with its own advantages and limitations. The most common energy flow topologies are [34]:

1. Adjacent cell-to-cell balancing: This topology involves transferring energy between adjacent cells in the battery pack. This is the simplest and most commonly used topology, but it can only balance cells that are adjacent to each other [35, 36].

2. Direct cell-to-cell balancing: This topology involves transferring energy between any two cells in the battery pack. This topology provides greater flexibility than adjacent cell-to-cell balancing but requires additional circuitry to enable energy transfer between non-adjacent cells [37, 38].

3. Cell-to-pack balancing: This topology involves transferring energy between individual cells and the entire battery pack. This topology is useful when the battery pack is composed of multiple sub-packs or when the cells are not easily accessible for direct energy transfer [32].

4. Pack-to-cell balancing: This topology involves transferring energy from a separate balancing pack to individual cells in the battery pack. This topology is useful when the battery pack does not have built-in balancing circuits, or when a separate balancing pack is needed to provide additional balancing capacity [39].

5. Cell-to-pack-to-cell balancing: This topology involves transferring energy between individual cells and the entire battery pack, but with an intermediate balancing circuit between the cells and the pack. This topology provides greater flexibility than cell-to-pack balancing but requires additional circuitry and may result in lower efficiency due to the additional conversion steps [40].

Each of these energy flow topologies has its own advantages and limitations, and the choice of topology will depend on the specific requirements of the battery system. The key factors to consider when selecting an energy flow topology for active cell balancing include the number of cells in the battery pack, the desired balancing accuracy, the available space and weight budget for the balancing circuits, and the overall cost and efficiency of the system.

2.5.2 Based on the Type of DC-DC Converter

DC-DC converters offer a wide range of operation with high flexibility and they are chosen for the present application based on the comparison of balancing method, energy flow, balancing speed/efficiency, size, cost, control complexity, and a maximum initial difference in SoC [3].

In addition, the number of circuit components, power rating, energy conversion efficiency, galvanic isolation, voltage conversion, and type of application, are some of the factors that are considered when choosing the type of converter [3].

- Non-isolated converters: These are the converters that transfer energy between input and output without providing galvanic isolation, which basically does not have a transformer and is simple, compact, and cost-effective.

  Buck-boost converters and quasi-resonant converters are more commonly used

in applications where galvanic isolation is not really critical or a requirement, such as automotive applications, telecommunications, and many more [41, 42].

- Isolated converters: Any conventional DC-DC converter which requires galvanic isolation to separate the input and output sides electrically. This is typically achieved by employing a transformer, where the energy transfers through magnetic coupling. These will also facilitate flexible grounding that fulfils the safety requirements, but there is a risk of being affected by high voltage applications.

Compared to the non-isolated converters, the isolated DC-DC converters tend to be more expensive, because of the existence of a transformer in the circuit and they also occupy more space.

Some of the most commonly used isolated converters are flyback converters, half-bridge converters, dual active converters, and push-pull converters. These types of converters are generally used in applications where isolation is crucial, such as energy storage systems, medical instruments/devices, industrial equipment, and photovoltaic applications [43, 44].

2.6 Battery Modeling

Battery cells are mainly composed of elements like anode, cathode, and electrolyte which raises the potential difference between them for the flow of electrons based on the electrochemical process. In order to understand the behaviors of the battery, it is necessary to build a model that captures the major static and dynamical properties.

The following subsections describe three different types of battery models, namely empirical models, electrochemical models, and equivalent circuit models.

2.6.1 Empirical Models

The empirical models are theoretical and numerically easy to use in designing and implementing BMS functions, but they do not offer insights into the internal behaviors of the battery. These internal behaviors provide important information that must be taken into account for both short- and long-term battery operations, such as the internal physical limitations and SoH of these batteries [45].

2.6.2 Electrochemical Model

An accurate prediction of the internal behaviors of the battery can be made using an electrochemical model, which is made up of complex, nonlinear partial differential-algebraic equations (PDAEs). This model, however, is inefficient in terms of computation [46]. As a result, reduced-order models such as lumped-parameter models (LPMs) or single-particle model are created, if and only if they are fine-tuned in

accordance with the electrolyte characteristics in thick electrodes and/or at high current rates. The LPMs are straightforward and call for less computational work. Some reduced-order models are derived as ordinary differential algebraic equations (DAEs), although it can be difficult to find a DAE solver that is computationally effective and numerically stable for real-time applications [47, 48].

2.6.3 Equivalent Circuit Model

In order to simulate and characterize the behavior of the battery cell with less computation, the equivalent circuit model is found to more advantageous over electrochemical models. The nonlinear electrochemical phenomenon inside the cell can be captured and simulated in system-level modeling.

Equivalent circuit models use electrical elements to capture and simulate the cell's static and dynamic characteristics. The mostly widely used equivalent circuit models include the first-order RC (1-RC) and second-order RC (2-RC) models, as shown in Figure 2.7 and Figure 2.8, respectively [49].

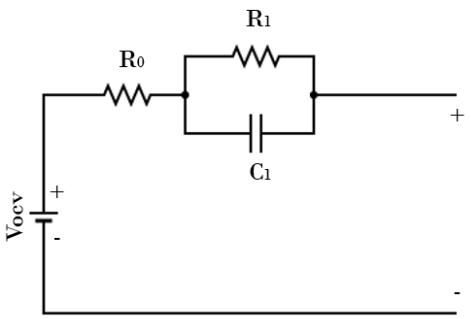

Figure 2.7: 1-RC circuit model.

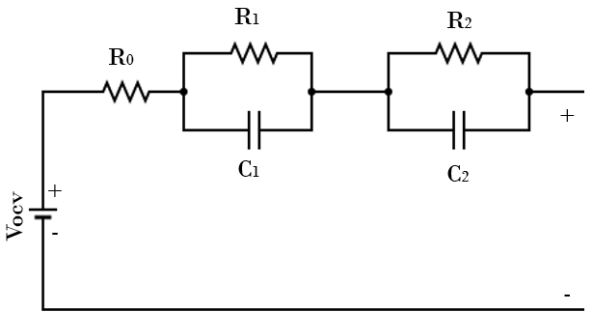

Figure 2.8: 2-RC circuit model.

The 1-RC and 2-RC equivalent circuit models capture the dynamic behaviors of the cell at different time scales. As shown in Figure 2.7 and Figure 2.8, R_o represents the internal resistance of the cell, and the voltage source V_{OCV} represents the open circuit voltage (OCV) across the cell. R_1 and R_2 capture the resistive effects due to the concentration or diffusion polarization, respectively [50, 51], and C_1 and C_2 are the polarization capacitance and diffusion capacitance that capture the transients, respectively [49].

2.7 SoC Estimation

SoC is expressed as the ratio of the unreleased capacity of the battery to its nominal capacity, which is always between 0 and 1. The fully charged cell is defined with SoC = 1, and the fully discharged cell with SoC = 0. However, in practical applications, the lower and upper SoC was usually maintained between 0.2 and 0.8 for the longevity of the battery and the battery control perspectives.

Mathematically, the cell's SoC at the given time instance t is calculated as the ratio of stored charge quantity Q_t to the nominal cell capacity Q_n, i.e., represented by

$$\mathrm{SoC}(t) = \frac{Q_t}{Q_n} \tag{2.1}$$

SoC estimation plays an important role in achieving an effective balancing process with the least possible errors. Also, accurate SoC estimation helps prolong battery life, prevent overcharging/overdischarging, and protect batteries from health/safety issues. Numerous techniques have been developed for SoC estimation, including the SoC-OCV method, the Coulomb counting method, and approaches based on electrochemical impedance spectroscopy (EIS). Also, some schemes are proposed using algorithms such as fuzzy logic (FL) and the Kalman filter (KF) family [3].

The standard KF can only be used for linear systems, where the SoC of the cell is dynamic and nonlinear in nature with respective to the measured voltage and cannot be directly applied for this application. However, there are methods like extended KF (EKF), adaptive EKF (AEKF), unscented KF (UKF), and ensemble Kalman filter (EnKF) using different filtering processes [3, 52].

2.8 Controllers

Controllers are the requisite devices that act as corrective tools for corresponding processes. Measured input signals are received and processed, and later output signals are generated and sent to actuators. Control accuracy, response time, and stability must be ensured in an optimal way [53].

Figure 2.9 presents the classification of control systems based on control loop and mode of operation which is discussed in the following sections.

2.8.1 Different Types of Control Loop

2.8.1.1 Open-Loop/Feedforward Control

In an open-loop system, where the input variable instructs a controller and the desired action is taken, the system establishes a desired relationship between the input of the plant and the set-point. The open-loop controller is independent of the regulated output variable, and the output will not be measured and compared to the target value; in other words, no feedback is established from the desired output. As a result, the open-loop system cannot adapt to model mismatches or external disturbances due to the varying environments [54].

As a simple example, a thermostat device is an open-loop control system which can be switched from ON to OFF status and vice versa depending on the predetermined temperature of the system.

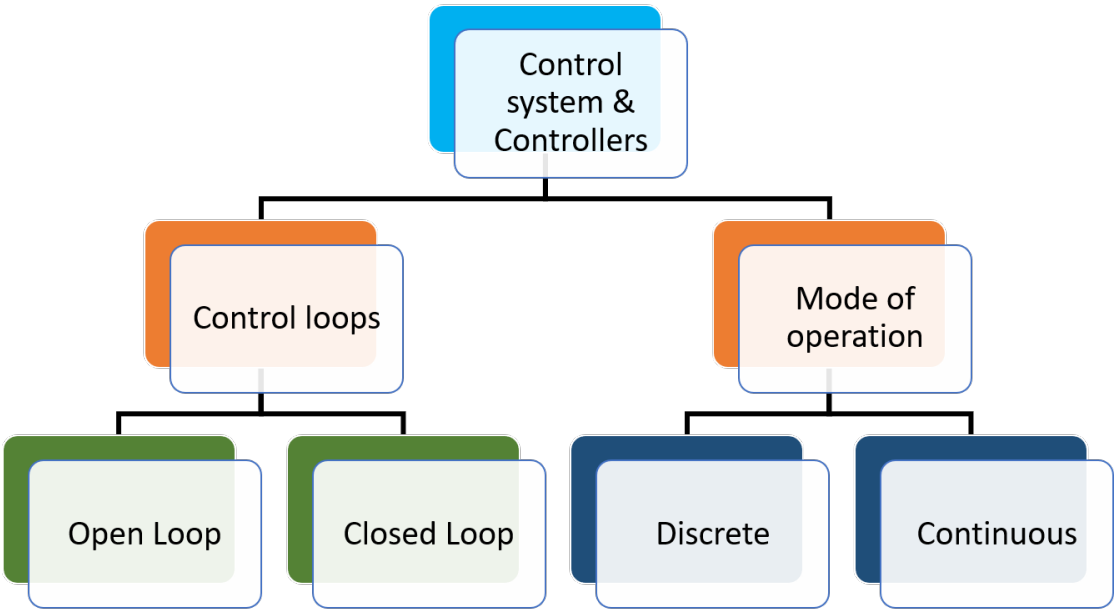

Figure 2.9: Types of controllers.

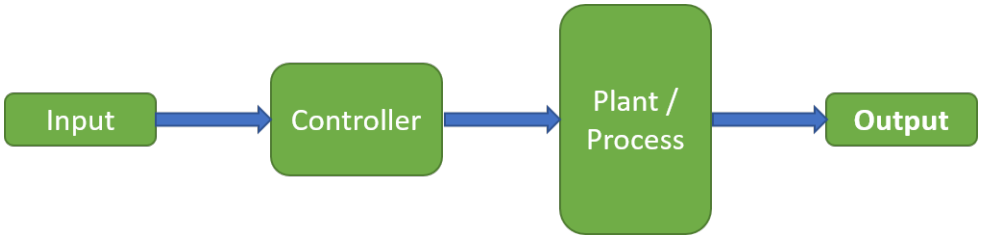

Figure 2.10: A simple open-loop control system [54].

A timer controller is another good example of an open-loop controller as the name implies that it controls the time to turn on and turn off the device at regular intervals [54].

Figure 2.10 represents a simple open-loop control system, where the system receives the reference input signal, adjusts the control signal, and obtains the corresponding output signal. The open-loop control is a low-cost and simple-to-implement technology. It is preferred when the system's output can be easily and reliably predicted by the model.

2.8.1.2 Closed-Loop/Feedback Control

Closed-control loops feature a cascaded system or feedback signals to help control the output variable. This system relies on a measured output variable that is processed by the controller, and the control signal is adjusted based on the difference between the the measurement and the reference/set-point. It attempts to reduce

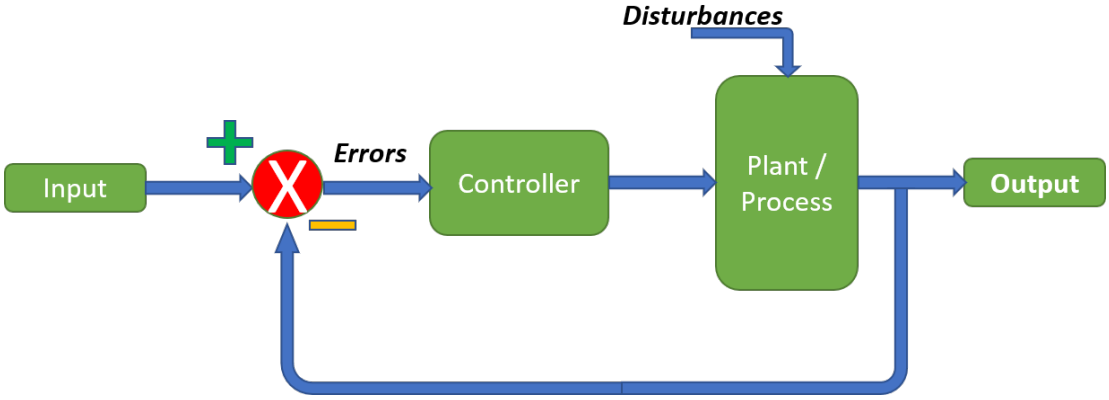

Figure 2.11: A simple closed-loop control system [55].

the degree of deviation in the system by making suitable adjustments in response to various disturbances, noises, or model mismatches [55].

Figure 2.11 illustrates a standard closed-loop control system where the output of the plant/process can be controlled according to the error between the output and the input reference (set-point).

2.8.2 Mode of Control Action

2.8.2.1 Discrete mode

Signals in discrete control systems change at specific times. A discrete control system's signals do not vary continuously in time. A discrete transfer function is used for representing the difference equation models in the frequency domain. One main disadvantage of the discrete control is that fine-grained changes may not be captured, and system precision is constrained when the time step is too large, while reducing the step size might significantly increase the computation.

2.8.2.2 Continuous mode

In this mode, continuous control signals are used. The controller uses transfer functions for differential equations. All potential values within a certain range can be represented by the continuous signals in such a continuous control system. Both the input and output are functions of time. However, the implementation of such a continuous control system can be costly due to its inherent complexity.

3

Methodology

This chapter presents the system models for the active cell balancing through the DC-DC converter. Section 3.1 presents different types of DC-DC converters and introduces their advantages and disadvantages. Section 3.2 compares these converters from the perspective of their performance parameters. Section 3.3 describes the balancing method and circuit. Sections 3.4 and 3.5 demonstrate a simple battery equivalent circuit model and its SoC estimation method. Section 3.6 describes the bidirectional buck-boost converter modeling using a state-space modeling approach and linearization. Section 3.7 is about modeling of PID controller for the balancing control.

3.1 Investigation of DC-DC Converter

DC-DC converters offer a wide range of operations and are chosen for the present application after considering factors such as energy flow, balancing speed/efficiency, size, cost, control complexity, and the maximum initial difference in SoC [3].

In addition, the number of circuit components, power rating, energy conversion efficiency, galvanic isolation, voltage conversion, and type of application, are some of the factors that are taken into account when choosing the type of converter [3].

3.1.1 Bidirectional Buck-Boost Converter

The bidirectional buck-boost converter is one of the most common converter types where the energy or the voltage can be stepped up or stepped down between the cells. The energy can be thus transferred between the cells through the DC-DC converter. This can be easily achieved by using the adjacent cell-to-cell (ACTC) type of balancing method [56, 57].

The buck-boost converter used in such a method consists of a power inductor to transfer the energy between the cells and the metal-oxide-semiconductor field-effect transistor (MOSFETs), which controls the duty cycle using pulse width modulation (PWM) signals [58]. For N cells connected in series, $N-1$ DC-DC converters are used to facilitate the balancing between the cells [3].

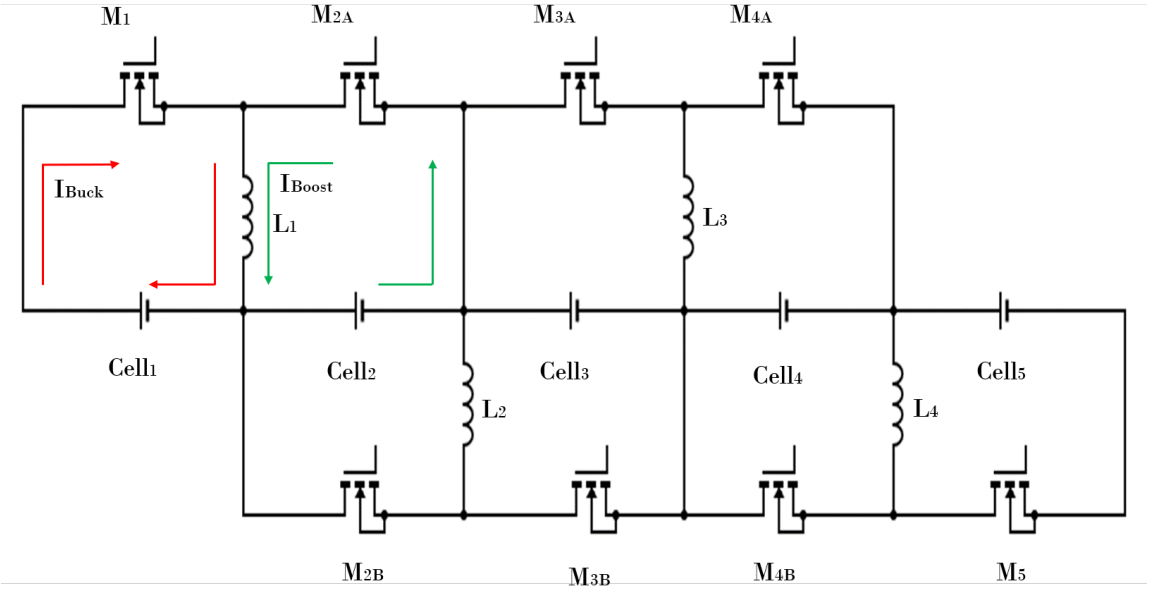

Figure 3.1: Schematic diagram of the bidirectional buck-boost converter.

3.1.1.1 Operation

As shown in Figure 3.1, a number of cells are connected in series along the buck-boost DC-DC converter. Consider the cells are in an imbalanced condition and the cells with higher SoC would transfer their charge to their neighbor cells with lower SoC. With well-designed control logic, cells will be balanced with certain balance accuracy [56]. For example, suppose the SoC of Cell 1 is higher than Cell 2. When the MOSFET M_1 is turned ON and M_{2A} is OFF, the energy will flow from Cell 1 to the power inductor L_1. Next, if the MOSFET M_1 becomes OFF state and M_{2A} is ON, the energy stored in the inductor L_1 will flow to Cell 2. The duty cycle of the MOSFET ON/OFF state is controlled by the duty ratio $D \in [0, 1]$, where the ON state refers to D and the OFF state refers to $1 - D$ [59].

3.1.1.2 Advantages

- Bidirectional operation: It can transfer energy in both directions, allowing for redistribution of charge between cells and equalizing the SoC among them [60].

- Wide voltage range and flexibility: The converter can handle a wide input and output voltage range and higher power conversion efficiency, making it suitable for balancing cells with varying voltage levels. It can be easily configured to adapt to different battery chemistries, cell capacities, and balancing requirements [61, 62].

- Compact size: Bidirectional buck-boost converters are typically compact, making them suitable for integration into BMS and various mobile applications [63].

- Cost-effectiveness: Leveraging existing technology, bidirectional buck-boost converters can be cost-effective compared to developing custom cell balancing solutions [3, 63].

- Efficiency: Bidirectional buck-boost converters are known for their high efficiency, minimizing power losses and maximizing overall system efficiency [3].

3.1.1.3 Disadvantages

- Efficiency at low loads: Efficiency may decrease at light loads. When the SoC difference between the adjacent cells is low, the balancing current becomes low, which increases the balancing time. This has a significant impact on the overall efficiency of cell balancing [3]. Additionally, in this ACTC-based method, only adjacent cells can be balanced together, leading to longer balancing time and decreased efficiency.

- Control complexity: If, for instance, the cells at the extreme ends are in an imbalanced state and the rest of them are in a balanced state, it needs to transfer the energy through all the cells from one end to another with this ACTC balancing topology. This also results in low conversion efficiency. Thus, Sophisticated control algorithms need to be developed for bidirectional power transfer in order to achieve accurate cell balancing, adding complexity to the system [64, 65].

3.1.2 Flyback Converter

The flyback converter is derived from the buck-boost converter, whereas the inductor is replaced with the transformer for the energy transfer between the cell. Flyback converters are more widely used in unidirectional or bidirectional energy-transferring modes such as PTC, CTP, and CTPTC balancing topology [3].

A flyback converter consists of a transformer with primary windings and secondary windings where the polarity of the secondaries is the opposite of the main winding. Also, the converter is constructed by connecting switches and diodes, and the MOSFET is controlled by the PWM signals [66, 67].

3.1.2.1 Operation

The operating principle of the flyback converter for active cell balancing is to transfer charge between cells to equalize their voltages or SoC by storing the energy in the form of the magnetic field in the transformer.

As the BMS continuously monitors the voltage levels of individual cells within the battery pack, it identifies cells with higher voltages and cells with lower voltages compared to the desired target voltage. Based on the voltage measurements, the BMS determines the amount of charge that needs to be transferred between cells

to achieve charge equalization. This information is used to control the operation of the flyback converter.

When the cell with a lower voltage needs to be balanced, the flyback converter operates in the charging mode. The primary side of the converter is connected to the higher voltage cell, while the secondary side is connected to the lower voltage cell, as shown in Figure 3.2 [66, 67].

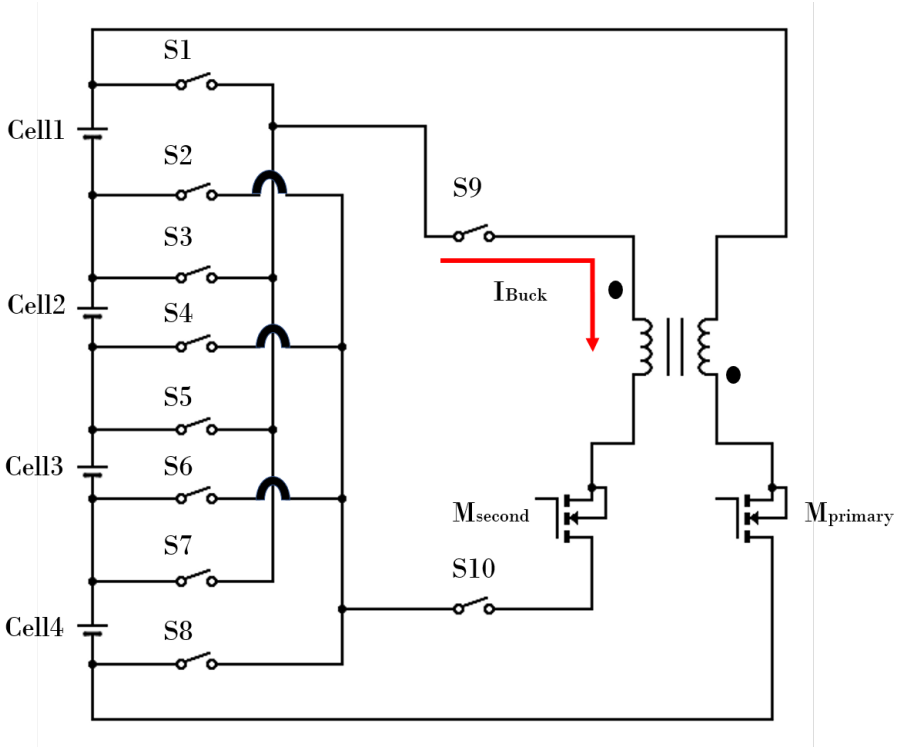

Figure 3.2: Schematic diagram of Flyback converter in buck mode.

When the primary side switch is turned ON, the energy is stored in the magnetic field of the transformer and when the primary side switch is turned OFF, the stored energy is transferred to the secondary side through the flyback action [66, 67].

Conversely, when a cell with higher voltage needs to be balanced, the flyback converter operates in the discharging mode. The primary side is connected to the lower voltage cell, and the secondary side is connected to the higher voltage cell. Energy is transferred the same way as in the charging mode, by operating the switches accordingly, as shown in Figure 3.3 [68].

Real-time control from BMS ensures accurate balancing and prevents overcharging or deep discharging of cells.

3.1.2.2 Advantages

- Electrical safety: Since the flyback converter consists of the transformer, it is considered as an isolated converter that can provide galvanic isolation. This

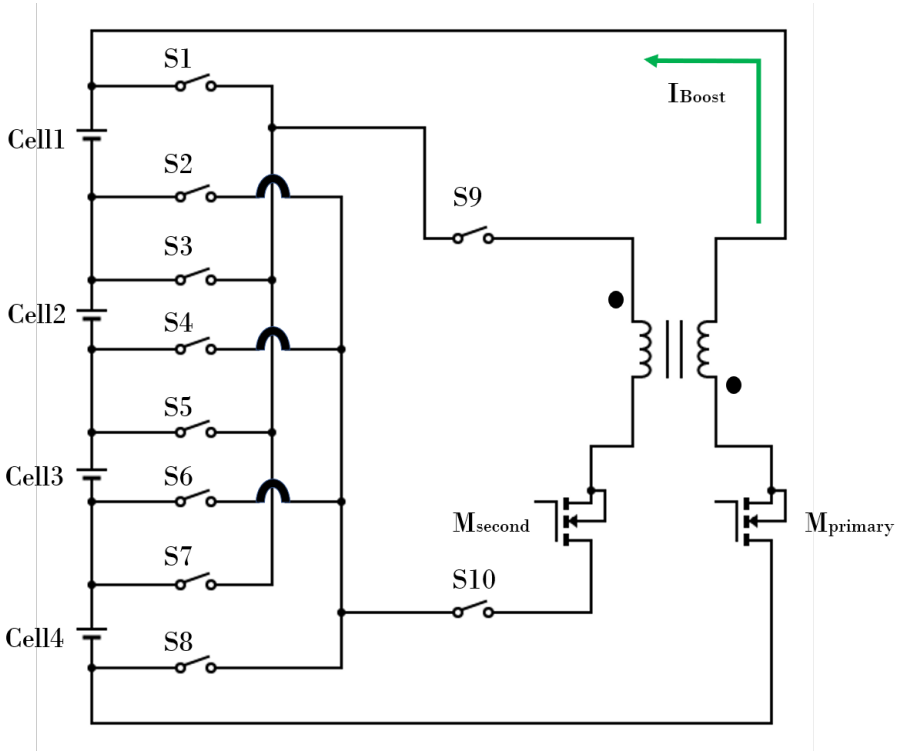

Figure 3.3: Schematic diagram of flyback converter in the boost mode.

isolation prevents the direct flow of electrical current between the input and output sides of the converter. It ensures the safety of the system and protects against electrical shocks, which is especially important in applications where the input and output voltages differ significantly, or when there is a need to protect sensitive components or operators from hazardous voltages [68].

- Scalability and energy flow: The bidirectional flyback converter can be easily scaled up or down to handle different battery pack sizes or power requirements. Also, it enables unidirectional and bidirectional energy transfer such as CTP, PTC, and CTPTC balancing methods [3, 69, 70].

3.1.2.3 Disadvantages

- Transformer design challenges and cost: Designing efficient and compact transformers for bidirectional flyback converters can be complex, necessitating careful consideration of factors such as leakage inductance, parasitic capacitance, and magnetic core selection. The transformer also increases the overall cost of the circuit [68].

- Voltage stress: The voltage stress across the semiconductor switches in bidirectional flyback converters can be relatively high, leading to increased power losses and reduced efficiency [68].

- Complex control and feedback: Bidirectional flyback converters require sophis-

ticated control algorithms and feedback mechanisms, making their implementation and fine-tuning challenging and requiring additional design efforts and expertise [67].

3.1.3 Dual Half-Bridge Converter

A half-bridge converter is a type of DC-DC converter that consists of two switches and a center-tapped transformer. It is widely used in power electronics applications for voltage step-up or step-down [3].

3.1.3.1 Operation

The dual half-bridge (DHB) converter consists of a transformer with high leakage inductance and one H-bridge that includes two switching elements on both sides of the transformer, as shown in Figure 3.4.

The transformer provides galvanic isolation and voltage synchronization between the LV and the HV sides. The energy is instantaneously stored in the leakage inductance of the transformer. DHB converters can be operated in both buck and boost modes. In this way, it was easily applied to PTC and CTP topologies [3].

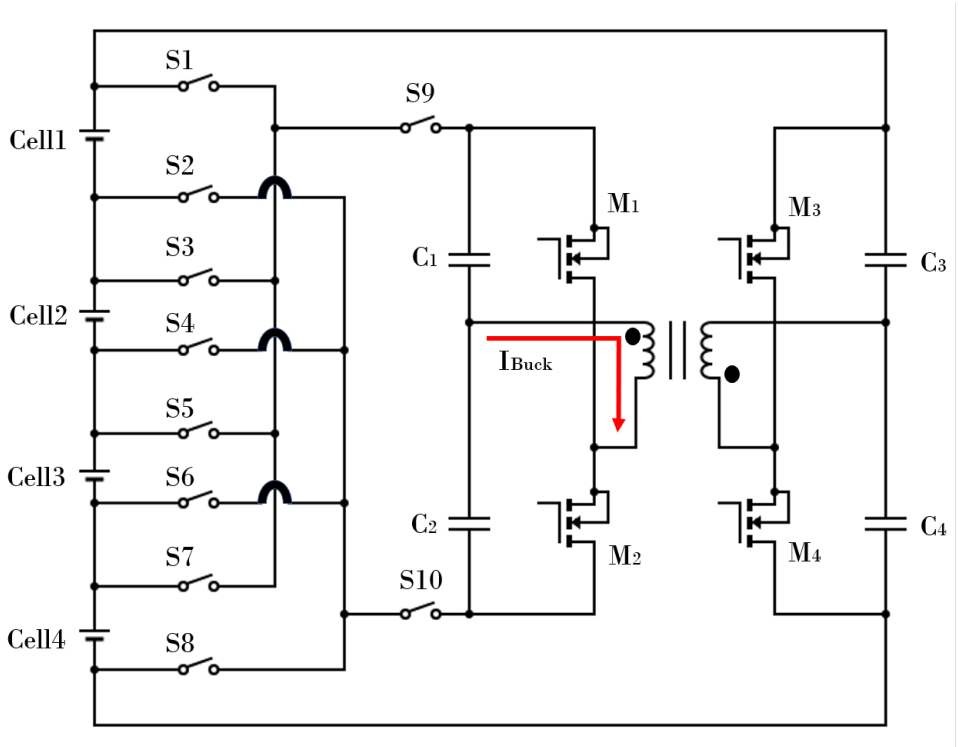

Figure 3.4: Schematic diagram of dual half-bridge converter in buck mode.

During operation, the half-bridge converter alternates between two states: the charging state and the discharging state. In the charging state, the switches on the primary side of the converter are controlled in such a way that the higher-voltage cells

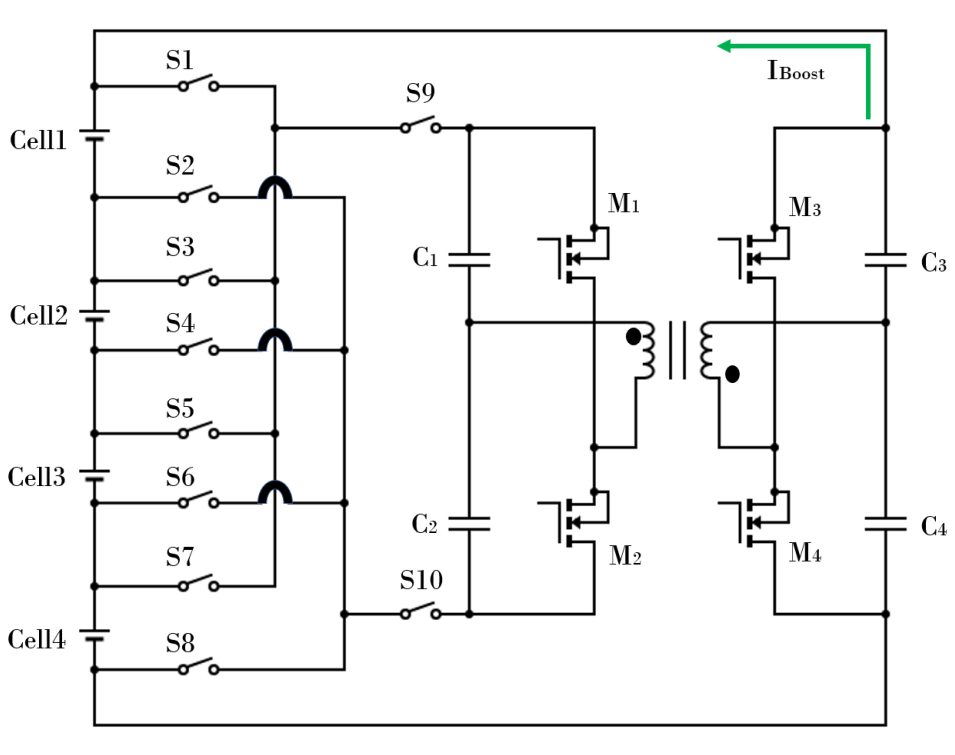

Figure 3.5: Schematic diagram of dual half-bridge converter in boost mode.

are connected in series, allowing them to transfer energy to the lower-voltage cells. This balancing process helps equalize the voltage levels among the battery cells [71, 72].

In the discharging state, as shown in Figure 3.5, the switches on the primary side are controlled differently, allowing the energy stored in the cells to be transferred to the load. The control circuitry continuously monitors the voltage levels of the cells and adjusts the switching pattern to maintain balanced cell voltages [73].

3.1.3.2 Advantages

- Active cell balancing in a half-bridge converter offers several advantages. By actively transferring energy between cells, it ensures that all cells contribute evenly to the power output, maximizing the overall capacity utilization of the battery pack. This balancing technique also promotes uniform aging among the cells, preventing premature failure of individual cells and extending the lifespan of the battery pack [71, 72].

- Reduction in switch voltage stress and reduced sizes of the transformer and inductor yield lower overall cost of the circuit and higher efficiency [71, 72].

3.1.3.3 Disadvantages

- It has increased weight as there is an inclusion of active cell balancing circuitry, along with the associated components like resistors, capacitors, inductors, and active switches. It increases the weight and size of the battery management system and also the overall cost of the system [71, 72].

- Longer balancing time and increased complexity: To achieve an efficient balancing system with the half-bridge converter, it requires additional control circuitry and monitoring algorithms to detect and balance the voltage or SoC of individual cells [3, 71, 72, 73].

3.2 Comparison of Different DC-DC Converters and Their Performance Parameters

Based on the system requirements and the implementation feasibility, the factors that influence the overall performance of the active cell balancing include the balancing method, efficiency, size, balancing speed, cost, control complexity, maximum initial SoC difference, etc [3].

For the selection of the type of converter and the balancing method to model and simulate the balancing, it is most important to study and compare the advantages and drawbacks of these influencing factors for the given converters. Table 5.1 is the decision matrix which provides a systematic approach to choose the type of converter and balancing method based on the application and control objective. This will be discussed in detail in the results Section 5.1.

3.3 Balancing Method and Balancing Circuit Design

Bidirectional energy flow between the cells provides an efficient way of shuffling the excessive energy and energizing the cells that are undercharged. With the selected type of buck-boost converter, the ACTC balancing method combines to drive the objective of cell balancing by transferring the energy between the adjacent cells. This is developed by using a systematic design approach for the circuitry involved in the system.

Figure 3.6 shows a circuit diagram of the cells and the balancing unit. This represents a battery module consisting of six cells connected in series, and the balancing circuit consists of a DC-DC converter for each adjacent pair of cells.

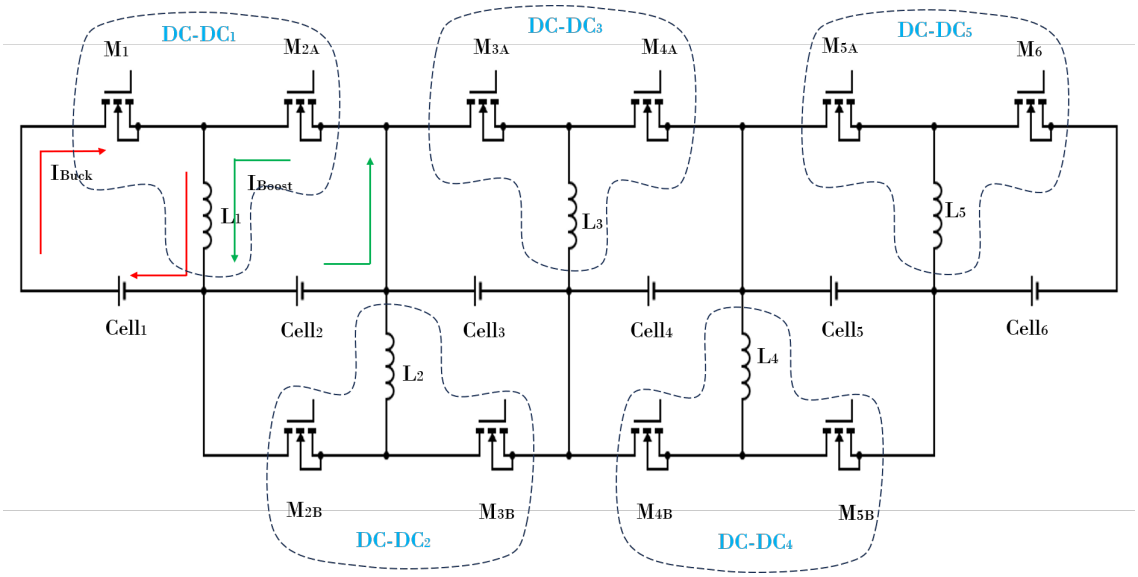

Figure 3.6: Circuit diagram of buck-boost converter balancing for six cells.

3.4 Battery Modeling

As shown in Figure 3.7, a constant voltage source connected with the resistor in series is the simplest battery cell model, where the resistor is used to capture the internal resistance of the cell and which is effective in analyzing any cell's dynamic performance.

In spite of their reduced accuracy compared to electrochemical/1RC/2RC models and their inability to effectively capture long-term parametric variations due to aging, the model in 3.7 is commonly adopted for control design due to their reduced computational costs and simplicity [48, 74].

In this thesis work, the model considered is a simple battery cell model with a voltage source (OCV shown in Figure 3.7) connected in series with the resister (R_0 shown in Figure 3.7) is just sufficient for designing and implementing control systems. Although the 1-RC and 2-RC equivalent models discussed in Section 2.6.3 offer better accuracy in modeling the charge transfer and lithium-ion diffusion processes, using a simpler model can reduce the complexity of the model and computation time for long time simulation. This terminal voltage of the battery is simply described by

$$V_{\text{bat}}(t) = \text{OCV}(\text{SoC}) + i_{\text{bat}}(t)R_0, \tag{3.1}$$

where i_{bat} is the current defined as positive during charging. The OCV is expressed as a nonlinear function of SoC and the estimation of SoC will be discussed in the next section.

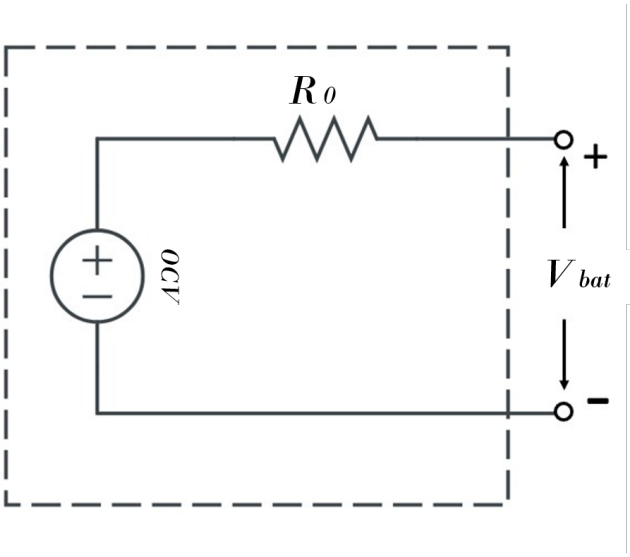

Figure 3.7: A simple battery equivalent circuit model.

3.5 Coulomb Counting Method for SoC Estimation

The input variables of the control system in the balancing process can be terminal voltage, OCV, SoC, or capacity. The performance indicators of the control system, such as stability and convergence, are directly dependent on the control parameters [3]. In this thesis work, the control parameter is considered to be SoC. Thus, the accurate and acceptable estimation of SoC is one of the necessary requirements. To minimize the complexity of the model, SoC estimation by the Coulomb counting method is considered, and this also facilitates achieving the required control accuracy provided that the initial condition or SoC is known.

In the coulomb counting method, the SoC at a given time t is estimated from the charging/discharging current at the given time $i_{\text{bat}}(t)$, which can be represented by

$$\text{SoC}(t) = \text{SoC}(0) + \frac{\eta}{3600 Q_n} \int i_{\text{bat}}(t) dt, \tag{3.2}$$

where SoC(0) is the initial value of SoC at $t = 0$, η is the coulombic efficiency, and Q_n defines the rated or nominal capacity of the battery.

Note that the accuracy of the coulomb counting method can be affected by wrong information of SoC(0), accumulating error of selected integration method and measurement noise of the current sensor, and inaccuracy capacity and efficiency. Advanced techniques such as those based on state observer/estimator or machine learning can be used to improve the SoC estimation but we will not elaborate these techniques.

3.6 Converter Modeling

3.6.1 State-Space Modeling for Buck-Boost Converter

The buck-boost converter with two ideal battery cells connected in series is modeled in this section by analyzing the converter's operating principle. As shown in Figure 3.8, the two cells are presented by two voltage sources (V_{in} and V_{out}) and two resistances (R_1 and R_2) located on the two sides of the converter, which correspond to the OCV and resistance R_0 as in Figure 3.7. While i_2 is defined in the same way as i_{bat} in (3.2), i_1 is the opposite of the corresponding battery current.

A general nonlinear state-space model can be expressed as

$$\dot{x} = f(x, u, u_d), \tag{3.3}$$

$$y = h(x, u, u_d), \tag{3.4}$$

where x is the state vector, $\dot{x}$ is the time derivative of state vector, u is the control input vector, u_d is the disturbance vector, and y is the output vector. f and h are two nonlinear operators for the system and output equations, respectively.

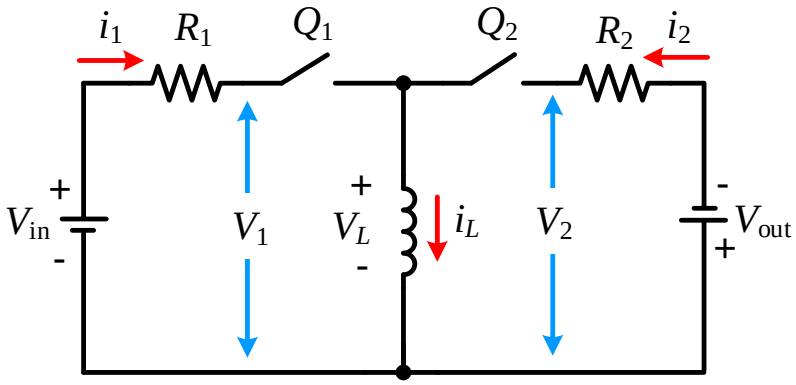

Figure 3.8: Buck-boost converter with two cells connected in series [75].

Table 3.1: Switching function for the MOSFETs and influencing variables.

D	Q1	Q2	V_L	i_2	i_1
D	1	0	V_1	0	i_L
$1-D$	0	1	$-V_2$	i_L	0

Table 3.1 shows the switching function for the MOSFETs and important variables such as the input/output currents and the inductor voltage, indicated in Figure 3.8 (The MOSFETs are represented as ideal switches). During the 'ON' state of the MOSFET Q1 during the duty cycle, D, the inductor will get charged through V_1 from Cell 1, and during the 'OFF' state of the MOSFET Q_1 or 'ON' state of MOSFET Q_2 during $1-D$, the inductor will get discharged leaving the current i_L to Cell 2,

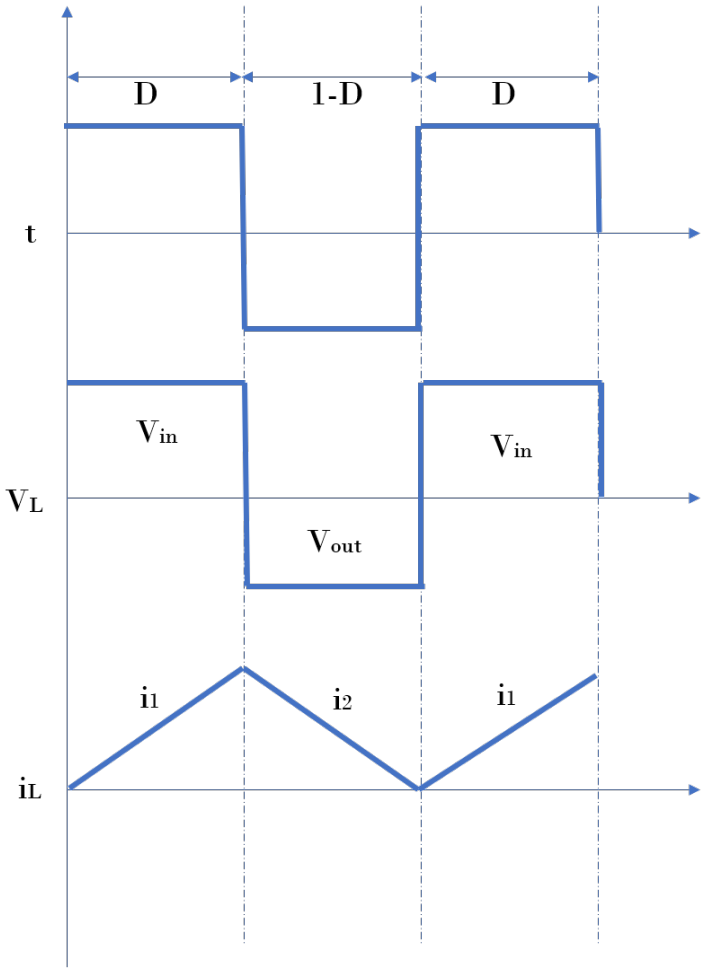

Figure 3.9: Graphical representation of PWM signal operating the MOSFETs.

and Figure 3.9 shows a graphical representation of PWM signals and corresponding response in voltages and currents. Applying Kirchhoff's laws for the loop 1 and 2 during the 'ON' and 'OFF' states, we can obtain the following averaged value model for the buck-boost converter:

$$L\frac{di_L}{dt} = V_L = DV_1 + (1-D)(-V_2), \tag{3.5}$$

$$V_1 = V_{\text{in}} - i_1 R_1, \tag{3.6}$$

$$V_2 = V_{\text{out}} + i_2 R_2, \tag{3.7}$$

$$i_1 = Di_L, \tag{3.8}$$

$$i_2 = (1-D)i_L. \tag{3.9}$$

Equations (3.5)–(3.9) represent the average-value model of the buck-boost converter and it can be represented using the equivalent circuit as shown in Figure 3.10. Note that the voltage source and the current source represent an ideal transformer component since the power on the two sides are equal.

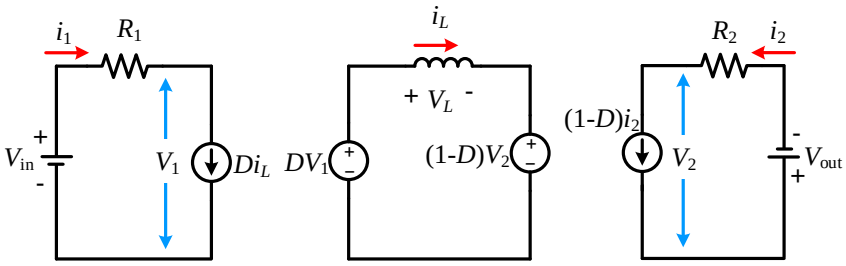

Figure 3.10: Equivalent circuit of the average model for the buck-boost converter with two cells connected in series.

The state-space equations for the buck-boost converter can be derived based on the circuit dynamics and Kirchhoff's laws while considering the state variables as below, where state vector only contains the inductor current i_L,

$$x = i_L.$$

The control input vector u is the duty cycle for the MOSFETs and the disturbance vector u_d consisting of the equivalent voltage sources and resistances of the batteries, e.g., V_{in}, V_{out}, R_1, and R_2, i.e.,

$$u = D, \quad u_d = \begin{bmatrix} u_{d,1} \\ u_{d,2} \\ u_{d,3} \\ u_{d,4} \end{bmatrix} = \begin{bmatrix} V_{\text{in}} \\ V_{\text{out}} \\ R_1 \\ R_2 \end{bmatrix}.$$

Thus, the nonlinear state equation that captures the dynamic behaviors of the buck-boost converter is

$$L\frac{dx}{dt} = (u_{d,1} - u \cdot x \cdot u_{d,3}) \cdot u - [u_{d,2} + (1-u) \cdot u_{d,4} \cdot x] \cdot (1-u). \tag{3.10}$$

We notice that for batteries, their voltages and resistances usually remain constant in the time frame for converter control. Thus, here we consider them to be fixed parameters instead of disturbances to simplify the state equation. This gives

$$\begin{aligned} L\frac{dx}{dt} &= (V_{\text{in}} - R_1 x \cdot u) \cdot u - [V_{\text{out}} + R_2 x \cdot (1-u)] \cdot (1-u) \\ &= -V_{\text{out}} - R_2 x + (V_{\text{in}} + V_{\text{out}} + 2R_2 x)u - (R_1 + R_2)xu^2. \end{aligned} \tag{3.11}$$

On the other hand, the output y contains the converter current and voltage. In this thesis, we select the output current i_2 and voltage V_2 as two variables to be controlled, i.e.,

$$y = \begin{bmatrix} y_1 \\ y_2 \end{bmatrix} = \begin{bmatrix} (1-u)x \\ V_{\text{out}} + R_2(1-u)x \end{bmatrix}. \tag{3.12}$$

It is worth noting that, by replacing the duty cycle D with the gating signal generated from the PWM, the above model becomes a switching function model in nature which can represent the high-frequency dynamics of the converter. This will be discussed more in Section 4.4.

3.6.2 Model Linearization

To control the voltage V_2 or the current i_2 of Cell 2, the duty cycle D is manipulated. Since the state-space model (3.11) and (3.12) are highly non-linear while in practical battery systems, a simple linear controller is desired for low-cost design and implementation, we shall linearize the model in this section for linear controller design.

Consider the converter's operation deviates from an operating/equilibrium point [76]. The model variables can be expressed by $x = x_0 + \hat{x}$, $u = u_0 + \hat{u}$, and $y = y_0 + \hat{y}$. where we assume that small perturbations indicated by the hat symbol are much smaller compared to equilibrium values denoted by the subscript "0". The nonlinear equations can be linearized as a small-signal model:

$$L\frac{d\hat{x}}{dt} = -[R_2(1-2u_0) + (R_1+R_2)u_0^2]\hat{x} + (V_{\text{in}} + V_{\text{out}} - 2R_1x_0)\hat{u}, \tag{3.13}$$

$$\hat{y}_1 = (1-u_0)\hat{x} - x_0\hat{u}, \tag{3.14}$$

$$\hat{y}_2 = R_2(1-u_0)\hat{x} - R_2x_0\hat{u}. \tag{3.15}$$

Equations (3.13)–(3.15) can be represented as a standard linear form of state-space equation:

$$\dot{x} = A\hat{x} + B\hat{u}, \tag{3.16}$$

$$\hat{y} = C\hat{x} + D\hat{u}, \tag{3.17}$$

where

$$A = -[R_2(1-2u_0) + (R_1+R_2)u_0^2]/L \tag{3.18}$$
$$B = (V_{\text{in}} + V_{\text{out}} - 2R_1x_0)/L \tag{3.19}$$
$$C = [(1-u_0), R_2(1-u_0)]^T \tag{3.20}$$
$$D = [-x_0, -R_2x_0]^T \tag{3.21}$$

The transfer function of the linearized model can be calculated by

$$G(s) = \begin{bmatrix} G_1(s) \\ G_2(s) \end{bmatrix} = C(sI - A)^{-1}B + D, \tag{3.22}$$

where G_1 is the transfer function between y_1 and u and $G_2 = R_2G_1$ is the transfer function between y_2 and u. This gives

$$G_1(s) = \frac{\hat{y}_1(s)}{\hat{u}(s)} = \frac{(1-u_0)(V_{\text{in}} + V_{\text{out}} - 2R_1x_0)/L}{s + [R_2(1-2u_0) + (R_1+R_2)u_0^2]/L} - x_0 \tag{3.23}$$

which can be rewritten as

$$G_1(s) = K_1\frac{1-\tau_1 s}{1+\tau_2 s} \tag{3.24}$$

where

$$K_1 = \frac{(1-u_0)(V_{\text{in}} + V_{\text{out}} - 2R_1x_0)}{R_2(1-2u_0) + (R_1+R_2)u_0^2} - x_0 \tag{3.25}$$

$$\tau_1 = \frac{L}{(1-u_0)(V_{\text{in}} + V_{\text{out}} - 2R_1x_0)/x_0 - [R_2(1-2u_0) + (R_1+R_2)u_0^2]} \tag{3.26}$$

$$\tau_2 = \frac{L}{R_2(1-2u_0) + (R_1+R_2)u_0^2} \tag{3.27}$$

Equation (3.24) represents a nonminimum phase system with a positive zero $s = 1/\tau_1$.

3.7 PID Controller

Feedback controllers generate the corrective action to alter the system input based on the deviation of the measured system output variable from the reference (i.e., set-point). This deviation is commonly known as the error, denoted by e. Below are several types of controllers which generate the control signal by applying gains (K_p, K_i, and K_d) with different operations on e.

- Proportional (P) controllers: The controller's output is proportional to the errors. A large proportional gain (K_p) tends to shorten the system's rise time and reduce the steady-state errors, but it may cause an increased overshoot and even system instability.

- Integral (I) controllers: The controller's output is generated based on the accumulation of the error over time. The integral gain (K_i) reduces the steady-state error and the rising time. The main drawback is that it increases both overshoot and settling time.

- Derivative (D) controllers: The output of the controller is produced proportional to the derivative of the error. It predicts the change of the error in the future, resulting in a faster response and improved stability. The derivative gain (K_d) can be used to reduce the system overshoot and the settling time.

- Proportional-integral-derivative (PID) controllers: PID controllers are highly sophisticated devices, and they are the most used controllers in the industry since they are cost-effective, easy to implement, simple to calibrate and provide excellent control performance.

Figure 3.11 shows a typical PID controller considered for achieving active cell balancing. The error signal/value $e(t)$ is the input to the PID controller, which is calculated as a difference between the set point $r(t)$ and the control variable $u(t)$ is being targeted to minimize the error value over time [78].

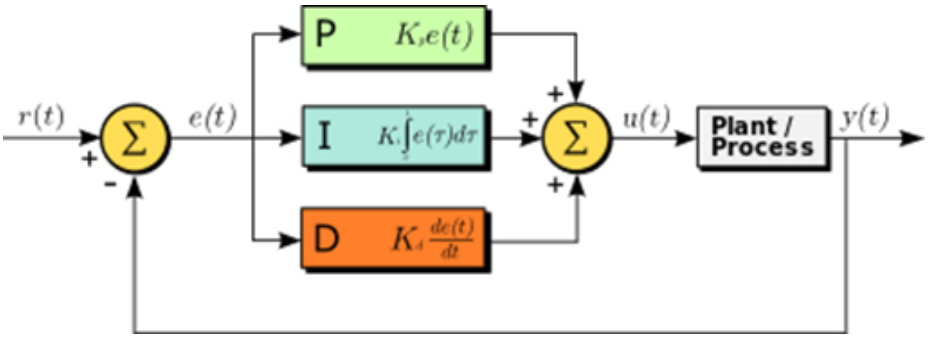

Figure 3.11: PID controller for active balancing [77].

The output of the PID controller can be expressed as

$$u(t) = K_p \cdot e(t) + K_i \cdot \int_0^t e(\tau)\, d\tau + K_d \cdot \frac{de(t)}{dt}. \tag{3.28}$$

Table 3.2: Effects of parameters in control response [78, 79].

Parameter	**Rise Time**	**Overshoot**	**Settling Time**	**Steady-State Error**
K_p	Decrease	Increases	Small change	Decrease
K_i	Decrease	Increases	Increases	Decrease
K_d	Small Change	Decrease	Decrease	No Change

Table 3.2 shows the influence of the control parameters of the PID controller on the response characteristics. Although a standard PID controller is formed by combining P, I, and D controllers, it is not necessary to employ all of them controllers in practice. How to configure the controller depends on the requirement of improvements that need to be made in the system. The selection of a good controller combination can ensure desired control performance with the simplest algorithm [77].

An efficient and reliable controller is tuned by comprehending the impact of PID gain settings utilizing the PID tuner and trial-and-error method. The response curve for the model is displayed in Figure 3.12.

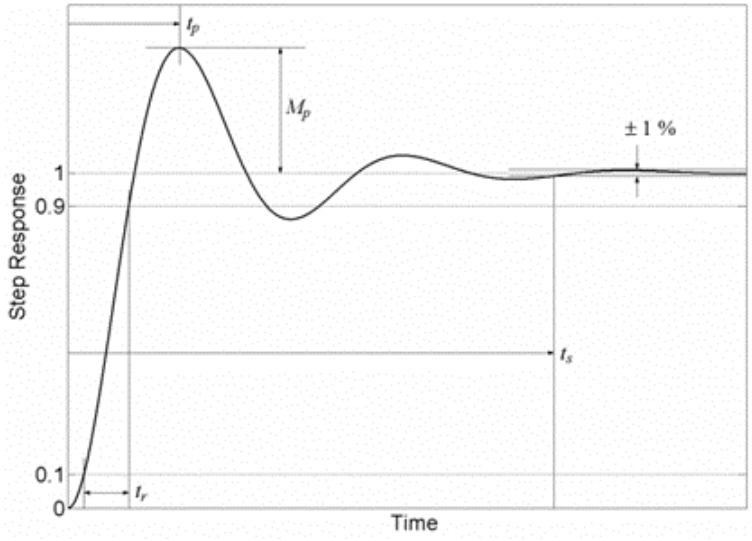

Figure 3.12: Typical response curve for a PID controller depicting the Rise time (t_p) Overshoot (M_p) and settling time (t_s).

4

Model Implementation

This chapter presents the implementation of the system model in MATLAB/Simulink using the Simscape toolbox. Section 4.1 presents the process flow of modeling the entire balancing system in Simulink. Section 4.2 describes the implementation of the battery model followed by SoC estimation using the Coulomb counting method in Section 4.3. Section 4.4 depicts the implementation of the buck-boost converter model of the balancing circuit. Section 4.5 discusses the PID controller for generating the PWM duty cycle. The development of the control algorithm is carried out in Section 4.6.

4.1 Process Flow of Modeling in Simulink

Simulink is one of the most common tools used for graphical modeling, simulating, and analyzing dynamical systems. In this thesis, Simulink has been used to develop the model, where the Simscape toolbox supports the modeling and simulation for various physical domains such as power systems, control systems, and many more. MATLAB has been used for the development of the control algorithm, which can be readily integrated with the Simulink model [80, 81].

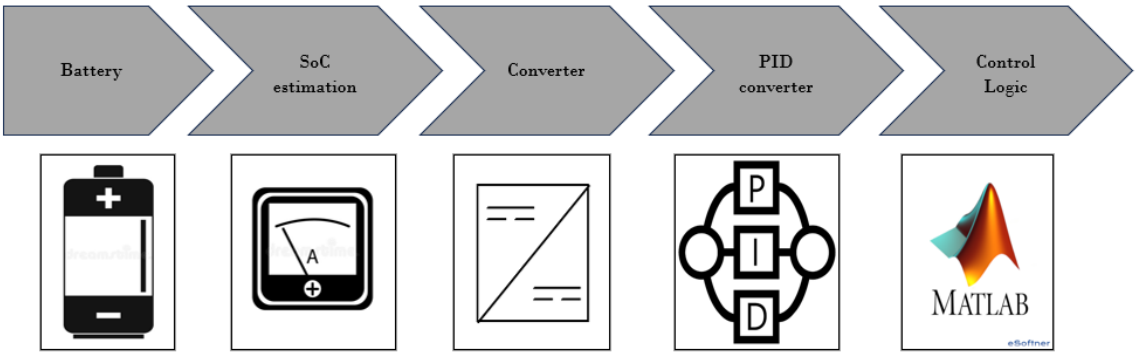

Figure 4.1: Modelling process flow for the balancing system.

Understanding and identifying the different subsystems and defining their requirements are the most important steps in developing a system-level model. The process flow of the modeling shown in Figure 4.1 visually describes the different subsystems involved, which technically supports planning the model architecture, searching for key Simulink blocks from the library, and their interconnections [82].

The flow illustrates the modeling carried out for each subsystem, namely, the battery model, DC-DC converter circuit modeling, SoC estimation, PID controller, and the control logic derived in Matlab script. In addition, the integration of these subsystems is demonstrated in the following sections to form the active cell balancing system for series-connected cells.

4.2 Battery Model

As discussed in Section 3.4, a simple circuit model, where the internal resistance R_0 is connected in series to the battery OCV (a controlled voltage source). The model parameters are from the specification of an industrial cell used for automotive applications, i.e., LG NCR18650, as shown in Table 4.1.

Table 4.1: Specifications for the typical industrial Li-ion cell considered in the battery modeling [83, 84, 85].

Nominal Capacity	3600 mAh
Nominal Voltage	3.63 V
Max. Charge Voltage	4.20 ± 0.05 V
Internal resistance, R_0	0.1 Ω [86]
Coulomb efficiency	96-99% [87]

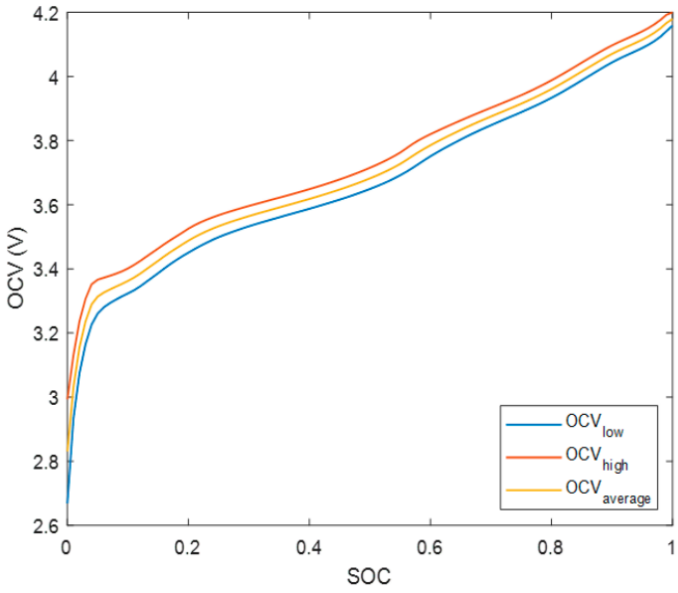

Figure 4.2: SoC–OCV curves for an NCA battery [86].

As shown in Figure 4.2, the upper OCV curve and the lower OCV curve refer to the measured voltage when the battery is charging or discharging using small currents, respectively. Averaging the two OCV curves yields the SoC-OCV curve used to calculate the OCV from the estimated SoC [86]. This relationship is used for all six cells, i.e., the differences between the OCV curves are not considered here.

4.3 SoC Estimation

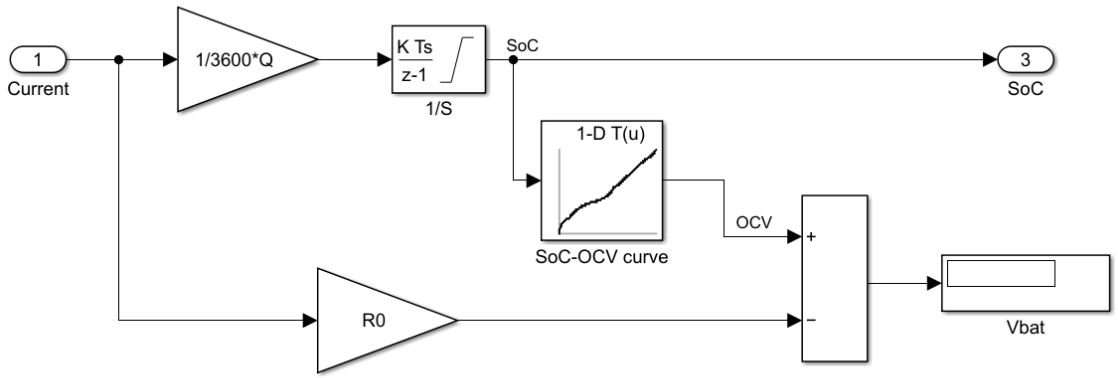

Figure 4.3: Battery model and SoC estimation.

The SoC estimation model implemented in Simulink is shown in Figure 4.3. The R_0 and Q are the internal resistance and the nominal capacity of the cell, respectively, and the applied current is the input variable to estimate the SoC of the cell. The initial SoC is assumed to be known. In addition, a look-up table containing the data of the SoC-OCV curve is used to calculate the OCV and then the terminal voltage of the cell.

4.4 Buck-Boost Converter Model

The detailed circuit model, average-value model, and the transfer function model of the buck-boost converter derived in Section 3.6 can both represent its dynamic behaviors. However, the transfer function model is highly idealized and only useful when the converter is working near a selected steady state. For the objective of simulating a practical circuit with non-ideal properties, we use the Simscape components to construct the average-value plant model. These include different passive elements, voltage and current sources, and measurement blocks. The average-value model is compared with the detailed model in Figure 4.4, where it can be seen that the average-value model can accurately reproduce the average component in the detailed model, and the high-frequency components due to the switching behaviors are ignored.

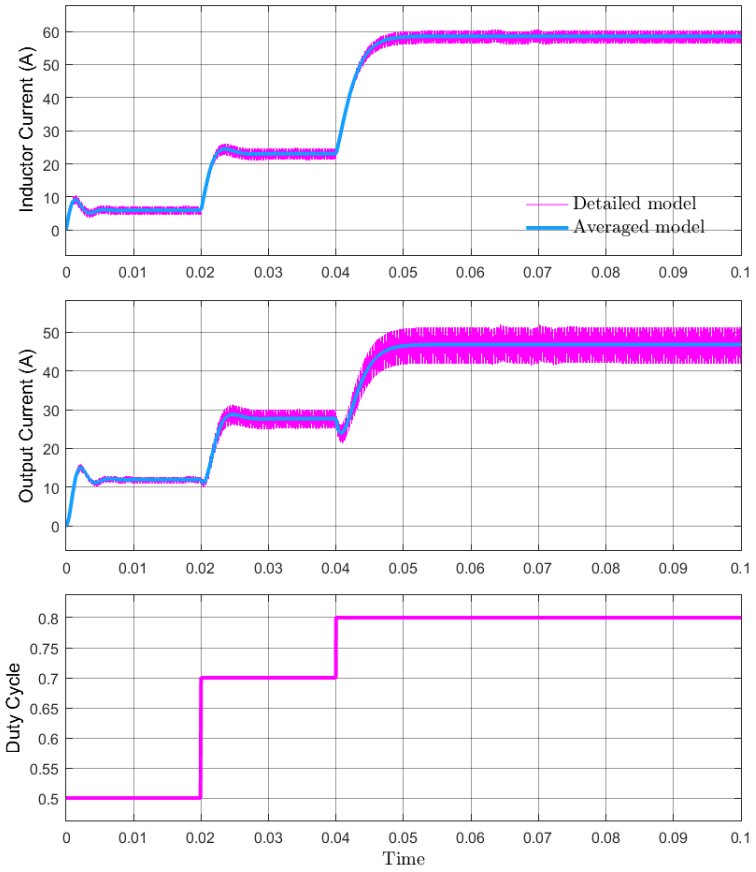

Figure 4.4: Comparison of the simulation waveforms using the detailed and average-value models of the buck-boost converter.

Figure 4.5 represents the converter model implemented in Simulink, using a switching logic to determine the duty cycle for the MOSFETs in the converter. As discussed in Section 3.6.1, the switching logic block was designed based on the switching function for the MOSFETs, which produces the input signal for the MOSFETs to operate according to the duty cycle received from the PID controller. However, the duty cycle received from the controller is the analog signal (D and $1-D$) that needed to be converted to a binary signal (0 or 1).

$$MOSFET\_1\_signal = PWM(DUTY\_1), \tag{4.1}$$

$$MOSFET\_2\_signal = \overline{PWM(DUTY\_1)}, \tag{4.2}$$

Equations (4.1)–(4.2) represent the logical expressions of the MOSFET signals as an output from the switching logic blocks denoted by $PWM()$, as illustrated in Figure A.1 in the appendix. In fact, with this switching logic, the average-value converter model is converted to a *switching function model* that represents the ideal switching behaviors of the MOSFETs.

Additionally, the ideal transformer block consists of a controlled current source and a controlled voltage source to form the ideal transformation of the voltage and current from Cell A, and similarly from Cell B.

From (3.5), the inductance of the converter can be determined by considering the maximum allowed current through it to be 25 A and the switching frequency of the MOSFETs to be 10 kHz. The inductance of the converter is directly proportional to the rate of change of current in the inductor and inversely proportional to the switching frequency. Hence, for the considered maximum balancing current, the inductance of the converter is chosen to be 2.5 mH [58, 61].

Cell balancing for two cells connected in series was constructed and is as shown in Figure 4.6. Cells A and B are constructed to be connected in series, and a buck-boost converter block is inserted between them according to the connections, with the necessary current and voltage sensors.

Upon validating the balancing procedure by simply initializing the imbalanced SoC for these two cells, the further design of the model can be developed for the n cells ($n = 6$ in this thesis).

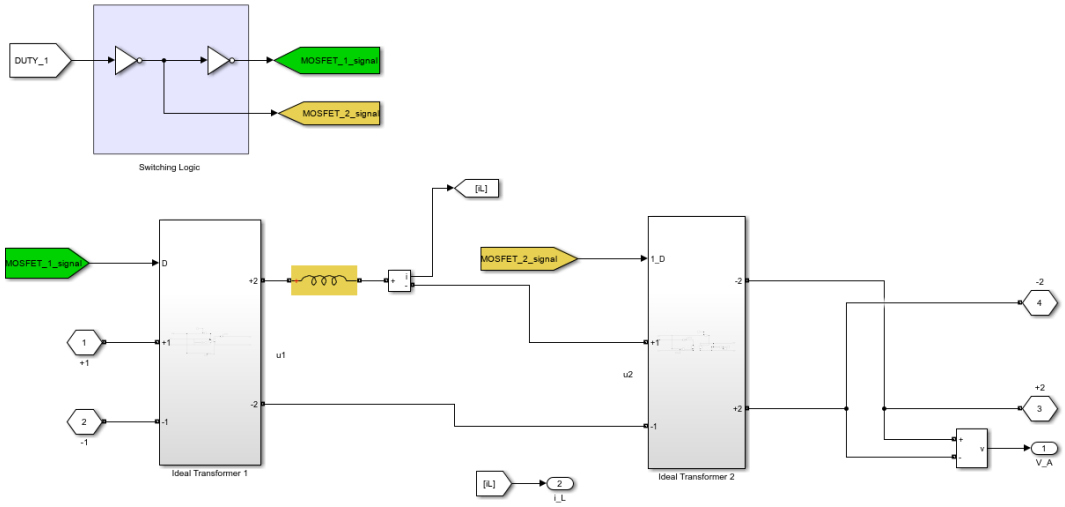

Figure 4.5: Buck-boost converter with switching logic in Simulink (a switching function model).

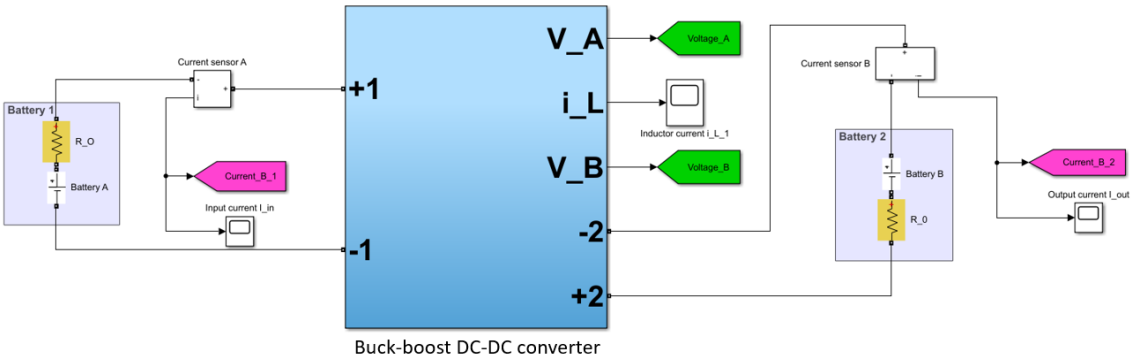

Figure 4.6: Cell balancing using a buck-boost converter for two cells connected in series in Simulink.

The duty cycles for pulse generator/PWM signal for the MOSFETs are based on the SoC levels of the cells, and the duty cycle for these is calculated in the switching logic, where it receives the SoC of all the cells, calculates the duty cycle ratio required to balance the cells in adjacent. This will be the input for the converter to balance the energy between each pair of adjacent cells.

In order to facilitate the energy flow between all six cells, one DC-DC converter has to be connected, which is discussed in Section 3.3.

4.5 PID Controller

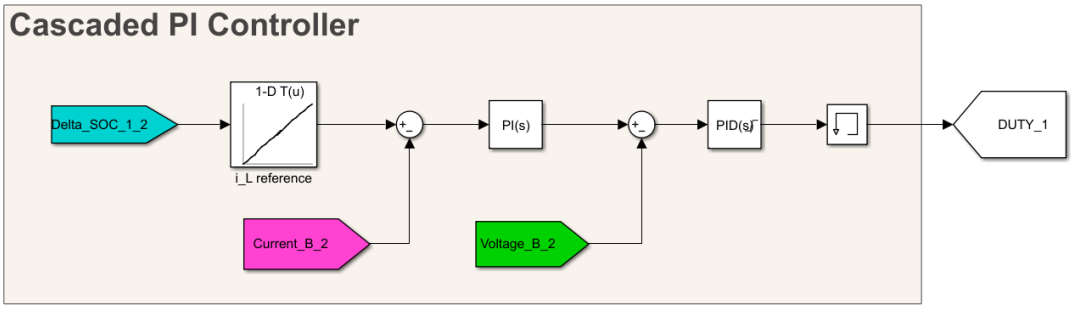

Figure 4.7: PID controller to control the PWM duty cycle.

Figure 4.7 represents the cascaded PI/PID controllers designed for generating the duty cycles. The control parameters discussed in Section 3.7 can be determined using different methods in order to optimize the system performance. Here, we utilize the built-in "PID tune" tool in Simulink for tuning the control parameters, which can auto-tune all the control parameters based on the plant under control, as illustrated in Figure A.2 in the appendix [88].

Commonly, active balancing is performed at relatively low C-rates, typically in the range of 0.1C to 0.5C [89]. Here, 'C' represents the capacity of the cell. The 1-D look-up table was constructed based on the considered 0.3 C-rate at which the balancing is initiated, where it receives the delta SoC of the adjacent cells and interpolates the balancing current required, which is then used as a reference or set-point for the controller. Also, the cell voltage and the balancing current are provided as the disturbance elements for the inner and the outer loops, respectively [90].

4.6 Control Algorithm

4.6.1 Maximum-SoC Difference Approach

In order to control the balancing process, the control algorithm was defined in the form of a mathematical expression where approaching a specified control law is necessary. In this thesis, the maximum-SoC difference approach was followed and programmed as a function in MATLAB, where the SoC of all the cells are the input signals and the switching logic concerned to a specific DC-DC converter is the output of the control algorithm.

The maximum-SoC difference approach considers the following principles;

- Calculate the difference in the SoC of the adjacent cells connected in series.
- Calculate the maximum differences of SoC of the adjacent cells.
- Prioritize the set of cells that has a maximum difference in SoC and initialize the switching logic for that DC-DC converter.

The control algorithm receives the dynamic values of the SoC according to the priority of the switching logic operation for the converter as output changes at the set frequency or discrete sample time of the simulation. This evaluation will be carried out until the defined SoC difference or the SoC balancing has been achieved in the cells and the balancing process exits the loop of the function once it is attained, as illustrated in Figure A.3 in the appendix.

5

Results

This chapter presents the results of the active cell balancing using a buck-boost converter. Section 5.1 discusses the choice of converter for the modeling and simulation in Simulink. Section 5.2 presents the results and analysis obtained from the simulation of the active cell balancing system.

5.1 Choice of Converter

According to the system requirements, technical assumptions, and limitations, this thesis work considers prioritizing the control complexity, balancing speed, and efficiency, while the size and the cost factors are not focused. The latter will be studied more in the future when realizing the developed model on hardware.

Table 5.1: Decision matrix for the selection of the type of converter and method [3].

Type of Converter	Buck-Boost Converter	Flyback Converter	Half-Bridge Converter
Balancing method	ACTC	CTPTC	CTP
Efficiency	Excellent	Good	Excellent
Size	Very high	Medium/High	Very high
Speed	Excellent	Excellent	Poor
Cost	Very high	High	Very high
Control complexity	Medium	High	Very high

Table 5.1 compares three types of converters in terms of corresponding balance method, efficiency, size, speed, cost, and control complexity. The drawbacks presented in Table 5.1 can vary depending on the system requirements. However, among these converters, the buck-boost converter is suitable for the purposes of modeling, design, and implementation. Thus, in this thesis, a bidirectional buck-boost converter operating in the ACTC mode is adopted.

5.2 Balancing Results and Analysis

5.2.1 Balancing the Evenly Imbalanced Cells

The Simulink model developed for the active cell balancing for six cells was used to evaluate the effectiveness by considering that the SoCs of the cells are evenly imbalanced. Figure 5.1 shows the initial imbalanced SoCs with a difference of 1% between adjacent cells, and thus the maximum initial SoC difference between all cells is 5%.

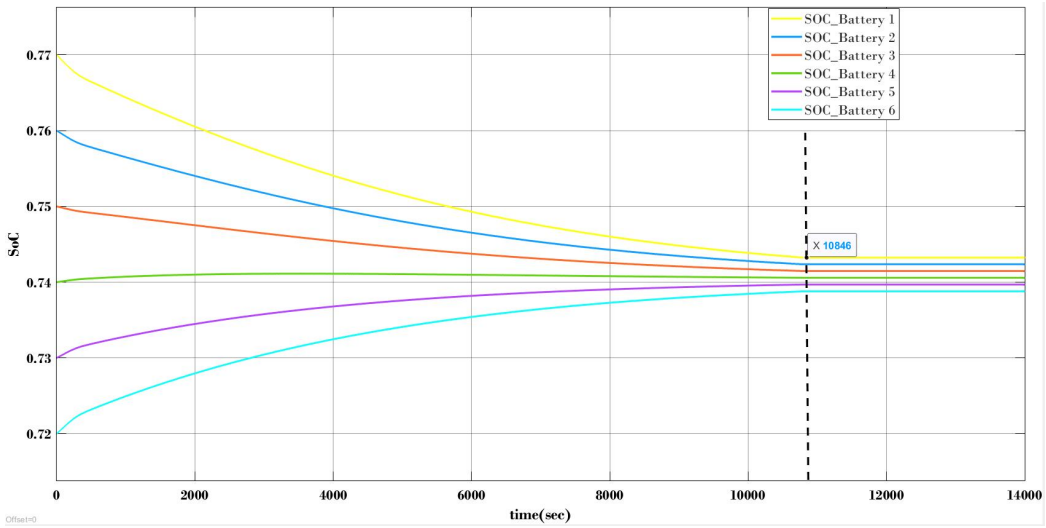

Figure 5.1: SoC of the cells balancing from 5% to 0.09 % imbalance difference.

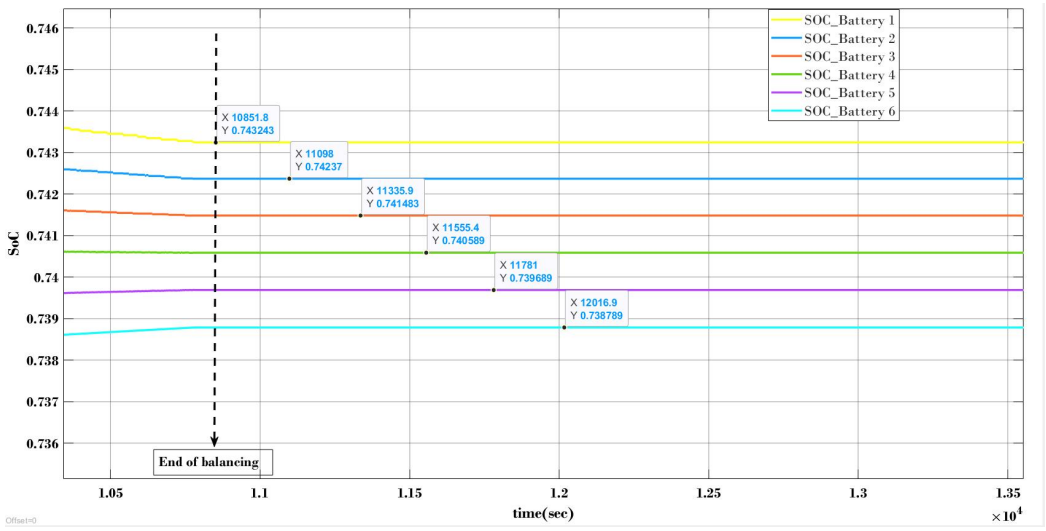

Figure 5.2: SoC at the end of balancing for the evenly-imbalanced cells.

Figures 5.1 and 5.2 present the balancing results in the given scenario, where the SoCs of the cells gradually converge to about the average value of all the cells. The control algorithm is designed by limiting the SoC difference after the balancing

process below a given threshold, e.g., 0.09% in this case, to guarantee a predefined precision, which reduces both the balancing time and the computation time. Since the cells considered in this case are equally imbalanced between the adjacent cells, during the balancing process, cells whose SoCs are higher than the average SoC release their energy, and the cells below the average SoC gain energy. The balancing process is considered completed after about 10,846 s, and the SoC differences between the adjacent cells are all successfully limited below 0.09%.

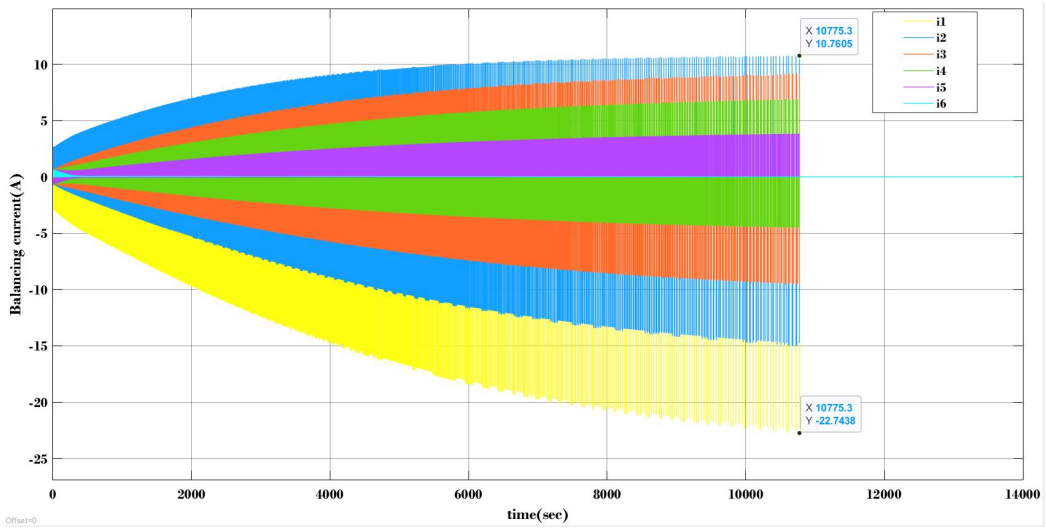

Figure 5.3: Balancing current of the cells in evenly-imbalanced states.

Figure 5.3 shows the balancing current, which is the charging or discharging current obtained as the result of the balancing process and the control algorithm discussed in Section 4.6.1. The maximum balancing current is 22.74 A in the discharging phase and 10.76 A in the charging phase.

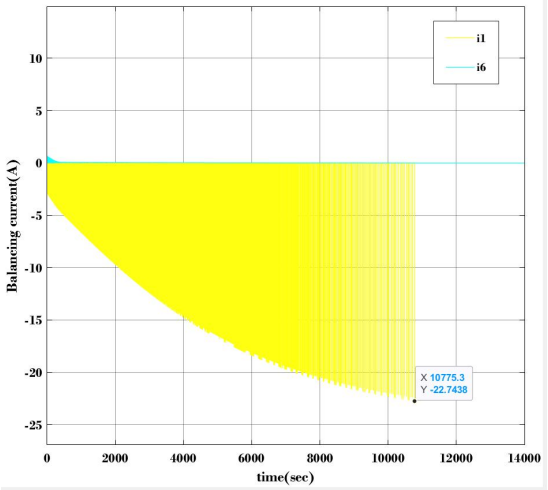

Figure 5.4: Balancing currents of Cells 1 and 6.

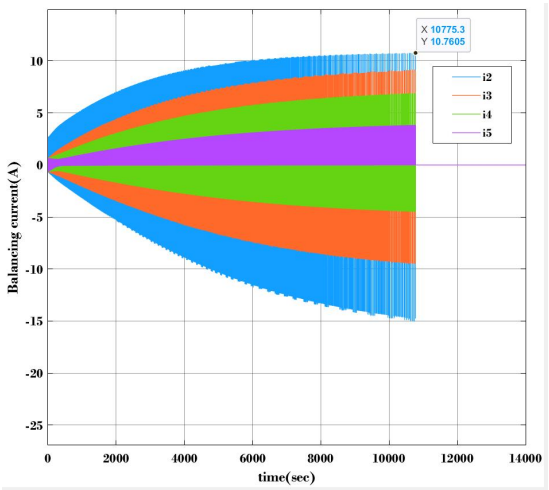

Figure 5.5: Balancing currents of Cells 2, 3, 4, and 5.

Figure 5.4 shows the balancing currents of Cells 1 and 6, which are obtained at the two ends of the circuit. The charge first moves from Cell 1 to its adjacent Cell 2,

and so on, based on the feedback control algorithm, until it is received by Cell 6 from its adjacent Cell 6.

In this process, Cells 2, 3, 4, and 5 need to be charged and discharged by exchanging charges with their adjacent cells to ensure the flow of energy/charge from high SoC cell to low SoC cell and vice versa, as shown in Figure 5.5.

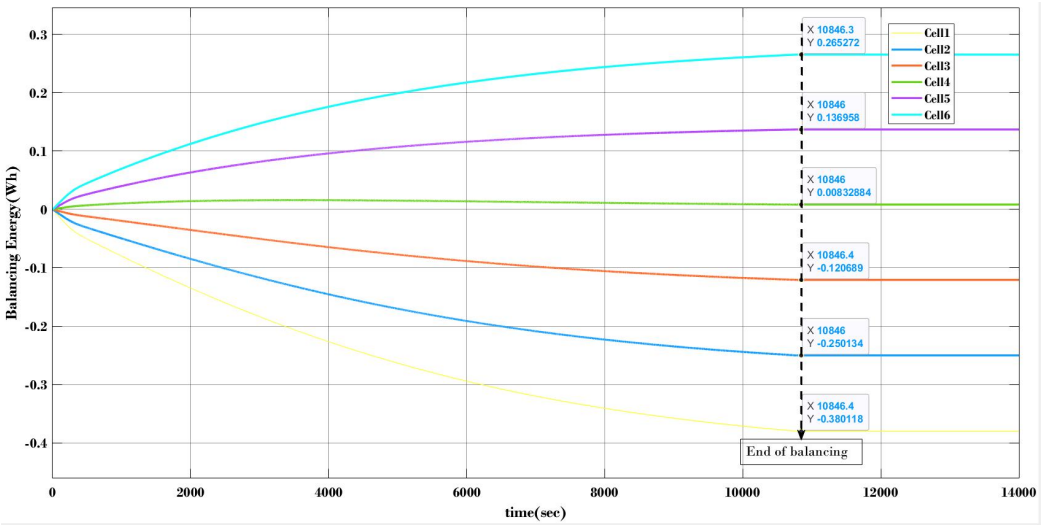

Figure 5.6: Balancing energy flow between evenly-imbalanced cells.

Table 5.2: Calculation of energy loss during balancing for evenly-imbalanced cells with reference to SoC and Energy plots.

Cell	Before balancing		After balancing (from SoC plot)		After balancing (from Energy plot)	
	SoC	Energy (Wh)	SoC	Energy (Wh)	Energy shuttled	Energy (Wh)
Cell 1	0.7700	9.1476	0.7432	8.8292	-0.3801	8.7675
Cell 2	0.7600	9.0288	0.7423	8.8185	-0.2501	8.7787
Cell 3	0.7500	8.91	0.7414	8.8078	-0.1206	8.7894
Cell 4	0.7400	8.7912	0.7405	8.7971	0.0083	8.7995
Cell 5	0.7300	8.6724	0.7396	8.7864	0.1369	8.8093
Cell 6	0.7200	8.5536	0.7387	8.7757	0.2652	8.8188
		53.1036		**52.8149**		**52.7632**
Energy Loss–>			0.2887 Wh		0.3404 Wh	
Energy Loss Percentage –>			0.5436 %		0.6410 %	

Figure 5.6 shows the energy plot derived by integrating the battery power over time, where power is calculated as the product of current and voltage for the cell. The computed energy loss is 0.3404 Wh, which is 0.6410% of total energy, as shown in Table 5.2. It also shows that the energy loss calculated from the SoC plot is 0.2887 Wh, which accounts for 0.5436% of the total energy. The energy loss is all from the battery's internal resistance, and the converter losses due to the resistance in the inductor and MOSFET components are not modeled.

5.2.2 Balancing the Randomly Imbalanced Cells

Simulations for the balancing were also carried out for more realistic scenarios where the initial SoCs are randomly distributed. The maximum initial SoC difference

between the cells is 9%.

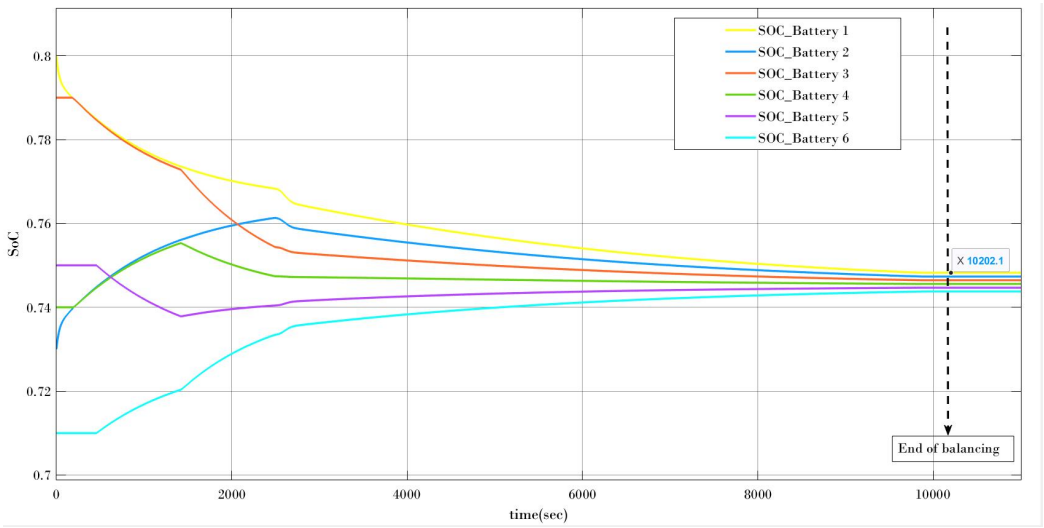

Figure 5.7: SoC of the cells balancing from 9% to 0.09% imbalance difference.

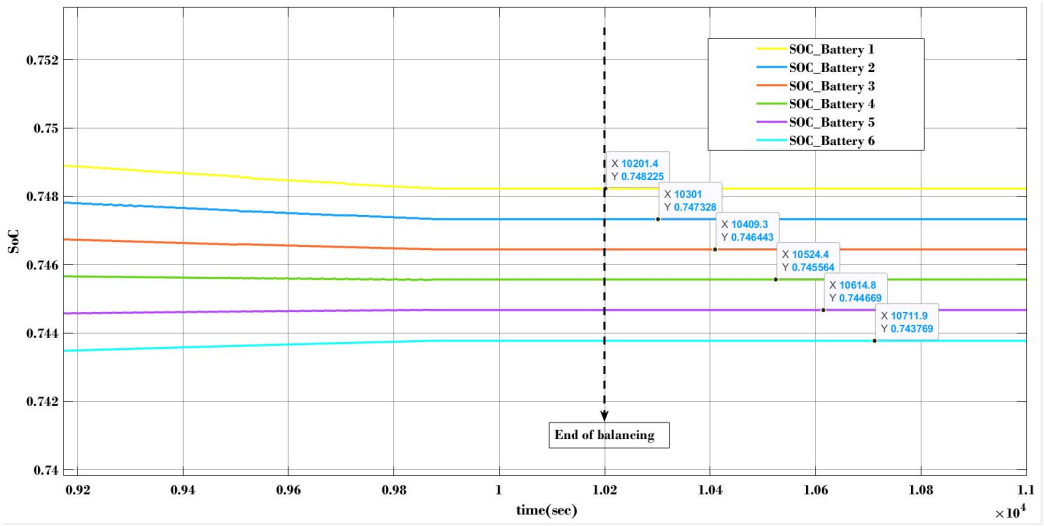

Figure 5.8: SoC at the end of balancing for randomly-imbalanced cells.

Figures 5.7 and 5.8 present the initial SoC of the cells and the behavior of the balancing process, where Cells 2, 4, and 5 are subjected to charge and discharge during balancing in order to reach their balanced states. This is because the energy is restricted to be transferred between the adjacent cells. The balancing process is terminated after about 10,202 s when the SoC difference between the cells has reached 0.09%.

Figure 5.9 presents the balancing current of the cells, where the maximum balancing current is observed to be 18.18 A and 10.02 A during the discharging and charging phases in the balancing process, respectively.

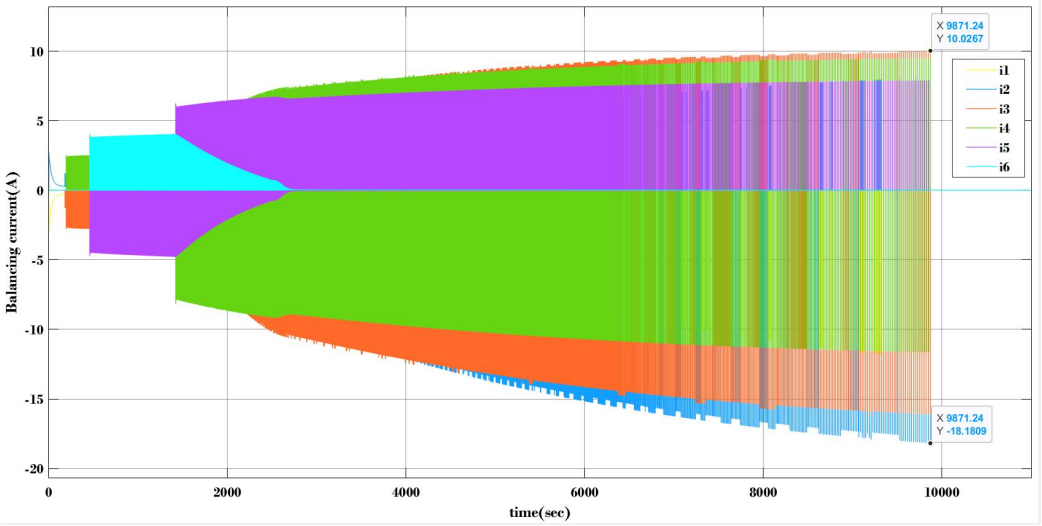

Figure 5.9: Balancing current of the cells in randomly-imbalanced states.

Figures 5.10 and 5.11 compare the balancing currents of Cell 5/Cell 6 and the balancing currents of Cell 4/Cell 5, respectively, in the same balancing process. It can be seen that these cells are not charging or discharging at the beginning. Cell 5 starts discharging its charge to Cell 6 at about 1408 s. After that, Cell 5 keeps receiving the charge/energy from Cell 4.

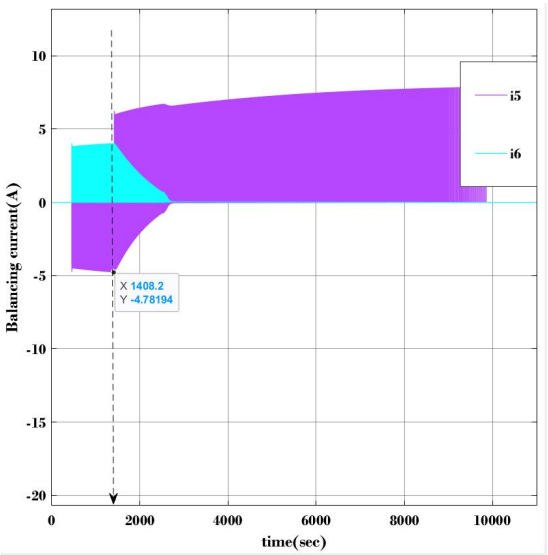

Figure 5.10: Balancing current flowing from Cell 5 to Cell 6.

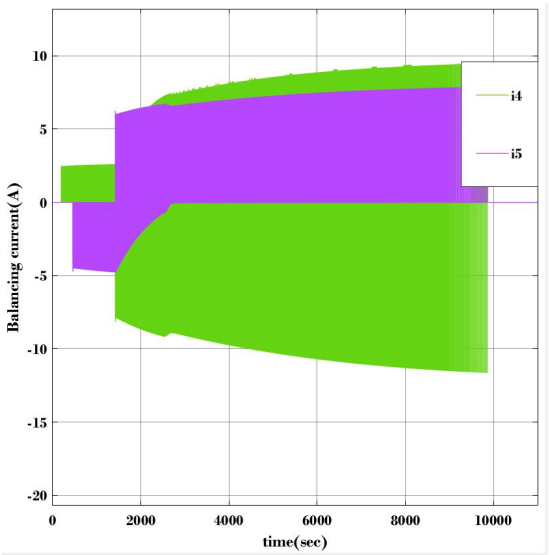

Figure 5.11: Balancing current flowing from Cell 4 to Cell 5.

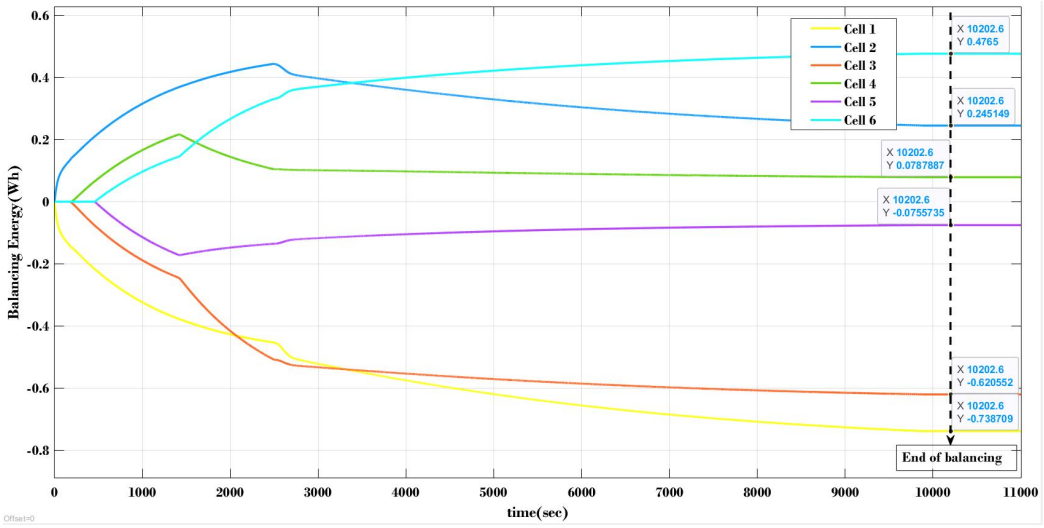

Figure 5.12: Balancing energy flow between randomly-imbalanced cells.

Table 5.3: Calculation of energy loss during balancing for randomly-imbalanced cells with reference to SoC and energy plots.

Cell	Before balancing		After balancing (from SoC plot)		After balancing(from Energy plot)	
	SoC	Energy (Wh)	SoC	Energy (Wh)	Energy shuttled	Energy (Wh)
Cell 1	0.8	9.504	0.7432	8.8886	-0.7387	8.7653
Cell 2	0.73	8.6724	0.7423	8.8779	0.2452	8.9176
Cell 3	0.79	9.3852	0.7414	8.8672	-0.6205	8.7647
Cell 4	0.74	8.7912	0.7405	8.8577	0.0787	8.8699
Cell 5	0.75	8.91	0.7396	8.8470	-0.0755	8.8345
Cell 6	0.71	8.4348	0.7387	8.8363	0.4765	8.9113
		53.6976		**53.1748**		**53.0633**
Energy Loss–>			0.5227 Wh		0.6343 Wh	
Energy Loss Percentage –>			0.9735 %		1.1812 %	

Figure 5.12 presents the energy flow between the cells during the balancing process. Table 5.3 summarizes the calculated energy losses. The energy loss is found to be 0.5227 Wh and 0.6343 Wh, corresponding to 0.97% and 1.18% in percentage, based on the SoC and energy, respectively.

6
Conclusion

This thesis starts with a comprehensive evaluation of different types of DC-DC converters for automotive applications in order to achieve enhanced system performance and prolonged battery longevity for electric vehicles.

Active cell balancing using DC-DC converters is increasingly important in research and development because of its high efficiency, high balancing speed, and superior robustness. Understanding the advantages and disadvantages of selected types of converters provided a solid base for choosing a converter for the concerned application. The bidirectional buck-boost converter, flyback converter, and dual half-bridge converter were analyzed for this purpose. The bidirectional buck-boost converter is considered better suited than the rest of the types, according to our evaluation.

A simple equivalent circuit model of batteries is used in this work, built in Simulink to depict the behavior of the battery cell's dynamic properties. For investigation, six cells are connected in series to form a battery module in the battery pack of an electric vehicle.

The Coulomb counting method is used to estimate the SoC of the cells and integrated into the model. The bidirectional buck-boost converter is initially designed and modeled to balance the energy or SoC between two adjacent cells. Upon validating the balancing process, the construction is carried out for the six cells. PID controllers are chosen and developed for the generation of the PWM signals for the MOSFETs in the converter because they are simple and easy to implement.

With the developed Simulink model, simulations are carried out under the scenarios with evenly imbalanced and randomly imbalanced SoC of the cells. In both cases, the cell-balancing model performed as expected, and it is observed that the balancing time is reasonably acceptable. At the same time, the energy efficiency is significantly improved over the objective comparison against the research work [3, 63]. A simple battery model, which reduced the complexity of the system, a PID controller, which allowed for enhanced control performance, and a robust control algorithm are contributing factors to these improvements.

The potential drawbacks and limitations of this method include the lack of thermal behaviors in the battery model, the SoH of the cells, and energy losses from the inductors. Furthermore, the balancing performance is tested only during the idle condition.

7
Future Work

We present the design and validation of a simple, effective model for active cell balancing using a DC-DC converter implemented in Simulink. The outcomes of the work were reasonable. However, there is potential to enhance the model's accuracy and the effectiveness of the balancing scheme by incorporating more sophisticated algorithms.

One suggestion is to adopt more detailed models, such as the 1-RC or 2-RC equivalent circuit models, which can capture a broader range of dynamic properties of the battery. These models would provide a more comprehensive foundation for improving the existing model. Furthermore, integrating a thermal model would offer a more precise insight into multi-physical battery behaviors, contributing to a more accurate overall system model. Including factors like the state of health (SoH) in the model would further enhance the model's predictive capabilities over a longer operation period.

Apart from the controllers discussed in Section 2.8, another suggestion is to explore advanced control approaches like model predictive control (MPC), adaptive control, fuzzy logic control, and optimal control. While these sophisticated techniques offer improved control performance, they may incur higher implementation costs including computation and storage resources. There is an opportunity to leverage artificial intelligence (AI) to simplify these advanced control methods.

To gain more insights of the balancing process and its optimal control strategy, it is recommended to consider various charging and discharging scenarios during the balancing process. This approach would contribute to a more realistic representation of the system's behavior.

Our last suggestion for future work would be to validate the model by implementing it on an actual hardware platform and comparing the results with the simulated outcomes in Simulink. This practical validation could provide valuable insights into the model's accuracy and effectiveness in real-world scenarios.

Bibliography

[1] H. Zakaria, M. Hamid, E. M. Abdellatif, and A. Imane, "Recent advancements and developments for electric vehicle technology," in *Proceedings of 2019 International Conference of Computer Science and Renewable Energies (ICCSRE)*, Agadir, Morocco, 2019, pp. 1–4. Available: https://doi.org/10.1109/ICCSRE.2019.8807726,

[2] M. A. Hannan, "State-of-the-art and energy management system of lithium-ion batteries in electric vehicle applications issues and recommendations," *IEEE Access* [Online]. vol. 6, pp. 19362–19365, Mar. 2018. Available: https://doi.org/10.1109/ACCESS.2018.2817655

[3] A. Turksoy, "A comprehensive overview of the dc-dc converter-based battery charge balancing methods in electric vehicles," *Renewable and Sustainable Energy Reviews* [Online]. vol. 133, pp. 1–17, Nov. 2020. Available: https://doi.org/10.1016/j.rser.2020.110274

[4] M. Dubarry, N. Vuillaume, and B. Y. Liaw, "Origins and accommodation of cell variations in Li-ion battery pack modeling," *International Journal of Energy Research* [Online]. vol. 34, no. 2, pp. 216–217, Dec. 2009. Available: http://dx.doi.org/10.1002/er.1668

[5] T. Baumhöfer, M. Brühl, S. Rothgang, and D. U. Sauer, "Production caused variation in capacity aging trend and correlation to initial cell performance," *Journal of Power Sources* [Online]. vol. 247, pp. 332–338, Feb. 2014. Available: https://doi.org/10.1016/j.jpowsour.2013.08.108

[6] S. Paul, C. Diegelmann, H. Kabza, and W. Tillmetz, "Analysis of ageing inhomogeneities in lithium-ion battery systems," *Journal of Power Sources* [Online]. vol. 239, pp. 642–650, Oct. 2013. Available: https://doi.org/10.1016/j.jpowsour.2013.01.068

[7] K.-C. Chiu, C.-H. Lin, S.-F. Yeh, Y.-H. Lin, C.-S. Huang, and K.-C. Chen, "Cycle life analysis of series connected lithium-ion batteries with temperature difference," *Journal of Power Sources* [Online]. vol. 263, pp. 75–84, Oct. 2014. Available: https://doi.org/10.1016/j.jpowsour.2014.04.034

[8] J. G.-Lozano, E. R.-Cadaval, M. I. M.-Montero, and M. A. G.-Martinez, "Battery equalization active methods," *Journal of Power Sources* [Online]. vol. 246, pp. 934–949, Jan. 2014. Available: https://doi.org/10.1016/j.jpowsour.2013.08.026

[9] Z. Wei, K. Liu, X. Liu, Y. Li, L. Du, and F. Gao, "Multi-level data-driven battery management: From internal sensing to big data utilization," *IEEE Transactions on Transportation Electrification*, vol. 9, no. 4, pp. 4805–4823, Dec. 2023. Available: https://doi.org/10.1109/TTE.2023.3301990

[10] M.A.Hannana, M.S.H.Lipub, A.Hussainb, and A.Mohamedb, "A review of lithium-ion battery state of charge estimation and management system in electric vehicle applications: challenges and recommendations," *Renewable and Sustainable Energy Reviews* [Online]. vol. 78, pp. 834–854, Oct. 2017. Available: https://doi.org/10.1016/j.rser.2017.05.001

[11] X. Jia, C. Zhang, Y. Li, C. Zou, L. Y. Wang, and X. Cai, "Knee-point-conscious battery aging trajectory prediction of lithium-ion based on physics-guided machine learning," *IEEE Transactions on Transportation Electrification* [Online] 2023. Available: https://doi.org/10.1109/TTE.2023.3266386

[12] W. C. Lee, D. Drury, and P. Mellor, "Comparison of passive cell balancing and active cell balancing for automotive batteries," in *IEEE Conference on Vehicle Power and Propulsion (VPPC)*, Chicago, IL, USA, 2011, pp. 1–7. https://doi.org/10.1109/VPPC.2011.6043108

[13] J. G.-Lozano, E. R.-Cadaval, M. I. M.-Montero, and M. A. G.-Martinez, "Battery equalization active methods," *Journal of Power Sources* [Online]. vol. 246, pp. 934–949, Jan. 2014. Available: https://doi.org/10.1016/j.jpowsour.2013.08.026

[14] D. Thakur, *Electric Vehicle Architecture & EV Powertrain Components* [Online]. Jul. 2021. Available: https://e-vehicleinfo.com/electric-vehicle-architecture-ev-powertrain-components/#:~:text=%2Dtolerant%2C%20safety.-,Electric%20Vehicle%20Architecture%20Powertrains,DC%2DDC%20converter%2C%20etc (visited on 22/02/2022).

[15] K. Medjdoub, A. Hazzab, B. Bouchiba, and M. Bendjima, "Fuzzy adaptive control for direct torque in electric vehicle," *International Journal of Power Electronics and Drive Systems (IJPEDS)* [Online]. vol. 4, pp. 557–566, Dec. 2014. Available: https://www.researchgate.net/publication/289064495_Fuzzy_adaptive_control_for_direct_torque_in_electric_vehicle

[16] Anon, *Circuit diagrams for EV vehicles* [Online]. 2009. Available: https://www.evworks.com.au/page/technical-information/ev-tech-info/

circuit-diagrams/ (visited on 22/02/2022).

[17] L. Schärtel, B. Reick, M. Pfeil, and R. Stetter, "Analysis and synthesis of architectures for automotive battery management systems," *Appl. Sci.* vol. 12, no. 21, pp. 1–24, Oct. 2022. Available: https://doi.org/10.3390/app122110756

[18] B. Ashok, K. Chidambaram, B. Mason, and S. D. Ashok, "Towards safer and smarter design for lithium-ion-battery-powered electric vehicles: A comprehensive review on control strategy architecture of battery management system," *Energies* [Online]. vol. 15, no. 12, pp. 3–44, Jun. 2022. Available: http://dx.doi.org/10.3390/en15124227

[19] N. Höök, "Database and modeling of field test data from lithium ion batteries in hybrid electrical vehicles," Master Programme in Engineering. Thesis, Dept. Physics, Uppsala University, Uppsala, 2011. http://uu.diva-portal.org/smash/record.jsf?searchId=8&pid=diva2%3A497894&dswid=6184

[20] Anon, *What is HMI?* [Online]. Aug. 2018. Available: https://inductiveautomation.com/resources/article/what-is-hmi (visited on 01/04/2022).

[21] M. Musielak, *What is an HMI, and why do we need it in the BMS?*. [Online]. April. 2020. Available: https://www.automatedbuildings.com/news/apr20/articles/gc5/200324031404gc5.html (visited on 01/04/2022).

[22] O. Kudalkar, *Communication within Battery Management system (BMS) and Different types of transmission(serial communication) modes with the help of real-time examples*. [Online]. Sep. 2021. Available: https://skill-lync.com/student-projects/communication-within-battery-management-system-bms-8051-microcontroller-archite (visited on 14/04/2022).

[23] R. Zhang, B. Xia, B. Li, and Y. Lai, "Study on the characteristics of a high capacity nickel manganese cobalt oxide (NMC) lithium-ion battery — an experimental investigation," *Energies*. vol. 11, no. 9, pp. 9–20, Aug. 2018. Available: http://dx.doi.org/10.3390/en11092275

[24] T. Huria, M. Ceraolo, J. Gazzarri, and R. Jackey, "High fidelity electrical model with thermal dependence for characterization and simulation of high power lithium battery cells," in *IEEE International Electric Vehicle Conference*, Greenville, SC, USA, 2012, pp. 2–7. Available: http://dx.doi.org/10.1109/IEVC.2012.6183271

[25] J. Qi, and D. D.-C. Lu, "Review of battery cell balancing techniques," in *Australasian Universities Power Engineering Conference (AUPEC)*, Perth, WA, Australia, 2014, pp. 2–5. Available:

https://doi.org/10.1109/AUPEC.2014.6966514

[26] M. Daowd, N. Omar, P. Van den Bossche, and J. Van Mierlo, "Capacitor based battery balancing system," *World Electric Vehicle Journal* [Online]. vol. 5, no. 2, pp. 385–393, Jun. 2012. Available: https://doi.org/10.3390/wevj5020385

[27] Ganesha N, G. Yadav, and Gowrishankara CK, "Analysis and implementation of inductor based active battery cell balancing topology," in *IEEE International Conference on Power Electronics, Drives and Energy Systems (PEDES)*, Jaipur, India, 2020, pp. 1–6. Available: https://doi.org/10.1109/PEDES49360.2020.9379358

[28] T. Duraisamy, and D. Kaliyaperumal, "Active cell balancing for electric vehicle battery management system," *International Journal of Power Electronics and Drive System (IJPEDS)* [Online]. vol. 11, no. 2, pp. 572–579, Jun. 2020. Available: http://doi.org/10.11591/ijpeds.v11.i2.pp571-579

[29] H. Sugumar, "Overview of cell balancing methods for Li-ion battery technology," *International Journal of Power Electronics and Drive System (IJPEDS)* [Online]. vol. 3, no. 2, pp. 1–12, Jul. 2020. Available: http://dx.doi.org/10.1002/est2.203

[30] M. Daowd, N. Omar, P. V. D. Bossche, and J. V. Mierlo, "Passive and active battery balancing comparison based on MATLAB simulation," in *IEEE Vehicle Power and Propulsion Conference*, Chicago, IL, USA, 2011, pp. 2–7. Available: https://doi.org/10.1109/VPPC.2011.6043010

[31] G.-Lozano J, R.-Cadaval E, M.-Montero MI, and G.- Martinez MA, "Battery equalization active methods," *Journal of Power Sources* [Online]. vol. 246, pp. 934–949, Jan. 2014. Available: https://doi.org/10.1016/j.jpowsour.2013.08.026

[32] A. M. Imtiaz and F. H. Khan, "Time shared flyback converter based regenerative cell balancing technique for series connected Li-ion battery strings," *IEEE Transactions on Power Electronics* [Online]. vol. 28, no. 12, pp. 5961–5967, Dec. 2013. Available: https://doi.org/10.1109/TPEL.2013.2257861

[33] S. S. Letha, Ravi D, P. Samuel, and B. M. Reddy, "Bidirectional dc to dc Converters: an overview of various topologies, switching schemes and control techniques," *International Journal of Engineering and Technology* [Online]. vol. 7, no. 5, pp. 361–362, Sep. 2018. Available: http://dx.doi.org/10.14419/ijet.v7i4.5.20107

[34] F. Baronti, R. Roncella, and R. Saletti, "Performance comparison of active balancing techniques for lithium-ion batteries," *Journal of*

Power Sources [Online]. vol. 267, pp. 603–609, Dec. 2014. Available: https://doi.org/10.1016/j.jpowsour.2014.05.007

[35] Q. Ouyang, J. Chen, J. Zheng, and H. Fang, "Optimal cell-to-cell balancing topology design for serially connected lithium-ion battery modules," *IEEE Transactions on Sustainable Energy* [Online]. vol. 9, no. 1, pp. 350–360, Jul. 2017. Available: https://doi.org/10.1109/TSTE.2017.2733342

[36] Y. Yuanmao, K. W. E. Cheng, and Y. P. B. Yeung, "Zero-current switching switched-capacitor zero-voltage-gap automatic equalization system for series battery string," *IEEE Transactions on Power Electronics* [Online]. vol. 27, no. 7, pp. 3234–3242, Jul. 2012. Available: https://doi.org/10.1109/TPEL.2011.2181868

[37] F. Baronti, G. Fantechi, R. Roncella, and R. Saletti, "High-efficiency digitally controlled charge equalizer for series-connected cells based on switching converter and super-capacitor," *IEEE Transactions on Industrial Informatics* [Online]. vol. 9, no. 2, pp. 139–1147, Oct. 2012. Available: https://doi.org/10.1109/TII.2012.2223479

[38] F. Mestrallet, L. Kerachev, J.-C. Crebier, and A. Collet, "Multiphase interleaved converter for lithium battery active balancing," *IEEE Transactions on Power Electronics* [Online]. vol. 29, no. 6, pp. 2474–2881, Aug. 2013. Available: https://doi.org/10.1109/TPEL.2013.2276152

[39] C.-H. Kim, M.-Y. Kim, H.-S. Park, and G.-W. Moon, "A modularized two-stage charge equalizer with cell selection switches for series-connected lithium-ion battery string in an HEV," *IEEE Transactions on Power Electronics* [Online]. vol. 27, no. 8, pp. 3764–3774, Jan. 2012. Available: https://doi.org/10.1109/TPEL.2012.2185248

[40] C.-H. Kim, M.-Y. Kim, H.-S. Park, and G.-W. Moon, "A modularized charge equalizer using a battery monitoring IC for series-connected li-ion battery strings in electric vehicles," *IEEE Transactions on Power Electronics* [Online]. vol. 28, no. 8, pp. 3779–3787, Nov. 2012. Available: https://doi.org/10.1109/TPEL.2012.2227810

[41] A. Bindra, *Non-Isolated Bus Converters Cut Cost, Improve Performance, Flexibility* [Online]. 2016. Available: https://www.digikey.com/en/articles/non-isolated-bus-converters-cut-cost-improve-performance-flexibility (visited on 28/06/2023)

[42] M. Salato, "Re-architecting 48V power systems with a novel non-isolated bus converter," in *IEEE International Telecommunications Energy Conference (INTELEC)*, Osaka, Japan, 2015. pp. 1–4. Available:

https://doi.org/10.1109/INTLEC.2015.7572441

[43] C. Wang, M. Li, Z. Ouyang, and G. Wang, "High efficiency high step-up isolated DC-DC converter for photovoltaic applications," in *IEEE Applied Power Electronics Conference and Exposition (APEC)*, Anaheim, CA, USA, 2019. pp. 1273–1280. Available: https://doi.org/10.1109/APEC.2019.8721916

[44] N. M. L. Tan, T. Abe, and H. Akagi, "Topology and application of bidirectional isolated DC-DC converters," in *8th International Conference on Power Electronics - ECCE Asia*, Jeju, Korea (South), 2011. pp. 1039–1046. Available: https://doi.org/10.1109/ICPE.2011.5944690

[45] N. A. Chaturvedi, R. Klein, J. Christensen, J. Ahmed, and A. Kojic, "Algorithms for advanced battery-management systems," *IEEE Control Systems Magazine* [Online]. vol. 30, no. 3, pp. 49–68, May. 2010. Available: https://doi.org/10.1109/MCS.2010.936293

[46] Y. Li, D. Karunathilake, D. M. Vilathgamuwa, Y. Mishra, T. W. Farrell, S. S. Choi, and C. Zou, "Model order reduction techniques for physics-based lithium-ion battery management: A survey," *IEEE Industrial Electronics Magazine*, vol. 16, no. 3, pp. 36–51, Sep. 2022. Available: https://doi.org/10.1109/MIE.2021.3100318

[47] Y. Li, M. Vilathgamuwa, T. Farrell, S. S. Choi, and N.T. Tran and J. Teague, "A physics-based distributed-parameter equivalent circuit model for lithium-ion batteries," *Electrochimica Acta* [Online]. vol. 299, pp. 451–469, Mar. 2019. Available: https://doi.org/10.1016/j.electacta.2018.12.167

[48] Y. Hu, S.Yurkovich, Y.Guezennec, and B.J.Yurkovich, "Electro-thermal battery modeling and identification for automotive applications," *Journal of Power Sources* [Online]. vol. 196, no. 1, pp. 449–457, Jan. 2011. Available: https://doi.org/10.1016/j.jpowsour.2010.06.037

[49] R. Zhang, B. Xia, B. Li, and Y. Lai, "Study on the characteristics of a high capacity nickel manganese cobalt oxide (NMC) lithium-ion battery - an experimental investigation," *Energies* [Online]. vol. 11, no. 9, pp. 2–20, Aug. 2018. Available: http://dx.doi.org/10.3390/en11092275

[50] S. Amir, M. Gulzar, M. O. Tarar, I. H. Naqvi, N. A. Zaffar, and M. G. Pecht, "Dynamic equivalent circuit model to estimate state-of-health of lithium-ion batteries," *IEEE Access* [Online]. vol. 10, pp. 18279–18288, Feb. 2022. Available: https://doi.org/10.1109/ACCESS.2022.3148528

[51] B. V. Rajanna, and M. K. Kumar, "Comparison of one and two time constant models for lithium ion battery," *International Journal of Electrical and Computer Engineering (IJECE)* [Online]. vol. 10, pp. 670–680, Feb. 2020.

Available: http://dx.doi.org/10.11591/ijece.v10i1.pp670-680

[52] Y. Li, B. Xiong, D. M. Vilathgamuwa, Z. Wei, C. Xie, and C. Zou, "Constrained ensemble Kalman filter for distributed electrochemical state estimation of lithium-ion batteries," *IEEE Transactions on Industrial Informatics* [Online]. vol. 17, no. 1, pp. 240–250, Feb. 2020. Available: https://doi.org/10.1109/TII.2020.2974907

[53] Anon. *Types of controller* [Online]. Available: https://electronicscoach.com/types-of-controllers.html (visited on 29/04/2022).

[54] Anon. *Open-loop Control System*. Available: https://electronicscoach.com/open-loop-control-system.html (visited on 29/04/2022).

[55] K. L. S. Sharma, "Overview of industrial process automation," *Automation Strategies* [Online]. pp. 54–62, 2011. Available: https://www.sciencedirect.com/science/article/pii/B9780124157798000061

[56] Y. Ma , P. Duan , Y. Sun, and H. Chen, "Equalization of lithium-ion battery pack based on fuzzy logic control in electric vehicle," *IEEE Transactions on Industrial Electronics* [Online]. vol. 65, no. 8, pp. 6762–6771, Jan. 2018. Available: https://doi.org/10.1109/TIE.2018.2795578

[57] K. Tytelmaier, O. Husev, O. Veligorskyi, and R. Yershov, "A review of non-isolated bidirectional dc-dc converters for energy storage systems," in *International Young Scientists Forum on Applied Physics and Engineering (YSF)*, Kharkiv, Ukraine, 2016, pp. 22–66. Available: https://doi.org/10.1109/YSF.2016.7753752

[58] T.-H. Wu, C.-S. Moo, and C.-H. Hou, "A battery power bank with series-connected buck–boost-type battery power modules," *Energies* [Online]. vol. 10, no. 5, pp. 2–12, Mar. 2017. Available: http://dx.doi.org/10.3390/en10050650

[59] J. F. Reynaud, C. E Carrejo, and C. Alonso, "Active balancing circuit for advanced lithium-ion batteries used in photovoltaic application," in *International Conference on Renewable Energies and Power Quality*, Las Palmas de Gran Canaria (Spain), 2011, pp. 1423–1428. Available: https://doi.org/10.24084/repqj09.682

[60] S. Yarlagadda, and T. T. Hartley, "A battery management system using an active charge equalization technique based on a DC/DC converter topology," *IEEE Transactions on Industry Applications* [Online]. vol. 49, no. 6, pp. 2720–2729, May. 2013. Available: https://doi.org/10.1109/TIA.2013.2264794

[61] S. Li, K. W. E. Cheng, Y. Ye, and Z. Shi, "Wide input and wide output topology analysis for tapped-inductor converters with consideration of parasitic elements," *IET Power Electronics* [Online]. vol. 9, no. 9, pp. 1952–1961, Jul. 2016. Available: https://doi.org/10.1049/iet-pel.2015.0591

[62] X. Wang, K. W. E. Cheng, and Y. C. Fong, "Non-equal voltage cell balancing for battery and super-capacitor source package management system using tapped inductor techniques," *Energies* [Online]. vol. 11, no. 5, pp. 2–12, Apr. 2018. Available: https://doi.org/10.3390/en11051037

[63] M.-Y. Kim, J.-H. Kim, and G.-W. Moon, "Center-cell concentration structure of a cell-to-cell balancing circuit with a reduced number of switches," *IEEE Transactions on Power Electronics* [Online]. vol. 29, no. 10, pp. 5285–5297, Nov. 2013. Available: https://doi.org/10.1109/TPEL.2013.2292078

[64] Q. Ouyang, J. Chen, J. Zheng, and Y. Hong, "SOC estimation-based quasi-sliding mode control for cell balancing in lithium-ion battery packs," *IEEE Transactions on Industrial Electronics* [Online], vol. 65, no. 4, pp. 3427–3436, Sep. 2017. Available: https://doi.org/10.1109/TIE.2017.2750629

[65] Y. Yuanmao, K. W. E. Cheng, and Y. P. B. Yeung, "Zero-current switching switched-capacitor zero-voltage-gap automatic equalization system for series battery string," *IEEE Transactions on Power Electronics* [Online]. vol. 27, no. 7, pp. 3234–3242, Dec. 2011. Available: https://doi.org/10.1109/TPEL.2011.2181868

[66] A. F. Moghaddam, and A. V. den Bossche, "Flyback converter balancing technique for lithium based batteries," in *8th International Conference on Modern Circuits and Systems Technologies (MOCAST)*, Thessaloniki, Greece, 2019, pp. 1–4. Available: https://doi.org/10.1109/MOCAST.2019.8741893

[67] M.-Y. Kim, J.-W. Kim, C.-H. Kim, S.-Y. Cho, and G.-W. Moon, "Automatic charge equalization circuit based on regulated voltage source for series connected lithium-ion batteries," in *8th International Conference on Power Electronics - ECCE Asia*, Jeju, Korea (South), 2011, pp. 2248–2255. Available: https://doi.org/10.1109/ICPE.2011.5944448

[68] Y.-Lin Lee, C.-H. Lin, and S.-J. Yang, "Power loss analysis and a control strategy of an active cell balancing system based on a bidirectional flyback converter," *Applied Sciences* [Online]. vol. 10, no. 12, pp. 2–17, Jun. 2020. Available: http://dx.doi.org/10.3390/app10124380

[69] X. Cui, W. Shen, Y. Zhang, C. Hub, and J. Zheng, "Novel active LiFePO4 battery balancing method based on chargeable and dischargeable capacity," *Computers & Chemical Engineering* [Online]. vol. 97, pp. 27–35, Feb. 2017.

Available: https://doi.org/10.1016/j.compchemeng.2016.11.014

[70] J.-W. Kim and J.-I. Ha, "Cell balancing method in flyback converter without cell selection switch of multi-winding transformer," *Journal of Electrical Engineering and Technology* [Online]. vol. 11, no. 2, pp. 367–376, 2016. Available: https://doi.org/10.5370/JEET.2016.11.2.367

[71] J. Sun, C. She, T. Cai, S. Duan, and C. Chen, "Analysis and modeling of dual-half-brige converter applied in high-voltage battery balancing," in *IEEE Energy Conversion Congress and Exposition (ECCE)*, Portland, OR, USA, 2018, pp. 2110–2114. Available: https://doi.org/10.1109/ECCE.2018.8558358

[72] B. Agrawal, M. Adam, B. Vadala, M. Koke, L. McCurlie, M. Preindl, R. Ahmed, and A. Emadi, "Non-dissipative battery cell balancing using half-bridge switching circuit," in *IEEE Transportation Electrification Conference and Expo (ITEC)*, Dearborn, MI, USA, 2016, pp. 1–6. Available: https://doi.org/10.1109/ITEC.2016.7520303

[73] K. Kim and H. Cha, "Dual-active-half-bridge converter with output voltage balancing scheme for bipolar DC distribution system," *IEEE Transactions on Industrial Electronics* [Online]. vol. 69, no. 7, pp. 6850–6858, Jul. 2021. Available: https://doi.org/10.1109/TIE.2021.3099233

[74] B. J. Yurkovich and Y. Guezennec, "Lithium ion dynamic battery pack model and simulation for automotive applications," in *ASME Dynamic Systems and Control Conference*, Hollywood, California, USA, 2009, pp. 241–248. Available: https://doi.org/10.1115/DSCC2009-2613

[75] R. H.G. Tan and L. Y. H. Hoo, "DC-DC converter modeling and simulation using state space approach," in *IEEE Conference on Energy Conversion (CENCON)*, Johor Bahru, Malaysia, 2016, pp. 42–47. Available: https://doi.org/10.1109/CENCON.2015.7409511

[76] M. R. Modabbernia, A. R. Sahab, M. T. Mirzaee, and K. Ghorbany, "The state space average model of buck- boost switching regulator including all of the system uncertainties," in *Advanced Materials Research*, Switzerland, 2011, pp. 3476–3483. Available: https://doi.org/10.4028/www.scientific.net/AMR.403-408.3476

[77] Wikipedia, *Proportional–integral–derivative controller* [Online]. 2019. Available: https://en.wikipedia.org/wiki/PID_controller (visited on 17/05/2022).

[78] Anon, *What is a PID Controller?* [Online]. 2018. Available: https://www.omega.com/en-us/resources/pid-controllers (visited

on 17/05/2022).

[79] Anon, *Introduction: PID Controller Design* [Online]. 2021. Available: https://ctms.engin.umich.edu/CTMS/index.php?example=Introduction&section=ControlPID (visited on 17/05/2022).

[80] The MathWorks, *Physical Modeling* [Online]. 2021. Available: https://www.mathworks.com/help/simscape/physical-modeling.html (visited on 14/03/2022).

[81] The MathWorks, *Basic Principles of Modeling Physical Networks* [Online]. 2021. Available: https://www.mathworks.com/help/simscape/ug/basic-principles-of-modeling-physical-networks.html (visited on 14/03/2022).

[82] The MathWorks, *Physical modelling with Simscape* [Online]. 2013. Available: https://www.mathworks.com/content/dam/mathworks/mathworks-dot-com/solutions/automotive/files/uk-expo-2013/physical-modelling-with-simscape.pdf

[83] Batemo GmbH, *Batemo Cell Library-Battery Specifications* [Online]. 2021. Available: https://www.batemo.de/products/batemo-cell-library/lg-chem-inr18650-m36/

[84] Akkuteile, *LG-INR18650M36 Battery Specifications* [Online]. 2022. Available: https://www.akkuteile.de/en/lg-inr18650-m36-3-6v-3-7v-3600mah-li-ion-positive-pole-raised_100819_2723

[85] LG Chem, *LG Chem. Product Specification* [Online]. 2017. Available: https://drive.google.com/file/d/1tq4b3GrzOFh1Aaf0hzuiAWVaOQdJBdBk/view

[86] M.-K. Tran, A. DaCosta, A. Mevawalla, S. Panchal, and M. Fowler, "Comparative study of equivalent circuit models performance in four common lithium-ion batteries: LFP, NMC, LMO, NCA," *Batteries* [Online]. vol. 7, no. 3, pp. 9–15, Jun. 2021. Available: https://doi.org/10.3390/batteries7030051

[87] F. Feng, R. Lu, and C. Zhu, "A combined state of charge estimation method for lithium-ion batteries used in a wide ambient temperature range," *Energies* [Online]. vol. 7, no. 5, pp. 3004–3032, May. 2014. Available: https://doi.org/10.3390/en7053004

[88] Anon,*Control System Basics* [Online]. 2022. Available: https://ledin.com/control-systems-basics/ (visited on 17/05/2022).

[89] S.-L. Wu, H.-C. Chen, and C.-H. Chien, "A novel active cell balancing circuit and charging strategy in lithium battery pack," *Energies* [Online]. vol. 12, no. 23, pp. 1–17, Nov. 2019. Available: https://doi.org/10.3390/en12234473

[90] The MathWorks, *Designing cascade control system with PI controllers* [Online]. 2019. Available: https://www.mathworks.com/help/control/ug/designing-cascade-control-system-with-pi-controllers.html (visited on 21/04/2022)

[91] *What is a PID Controller : Working & Its Applications* [Online]. Available: https://www.elprocus.com/the-working-of-a-pid-controller/ (visited on 17/05/2022).

A

Appendix 1

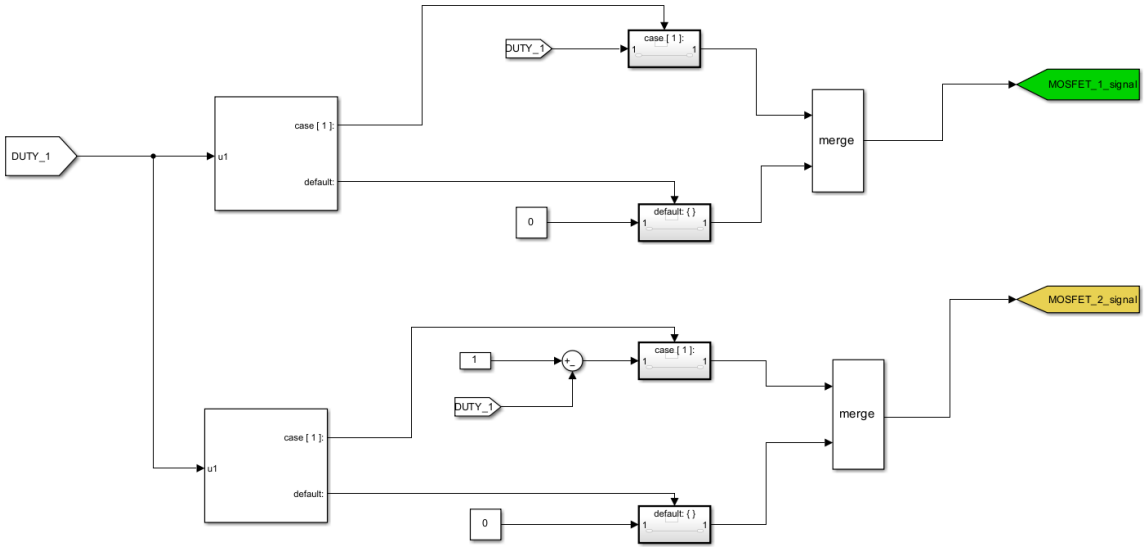

Figure A.1: Switching logic block that produces input for the MOSFETs in Simulink

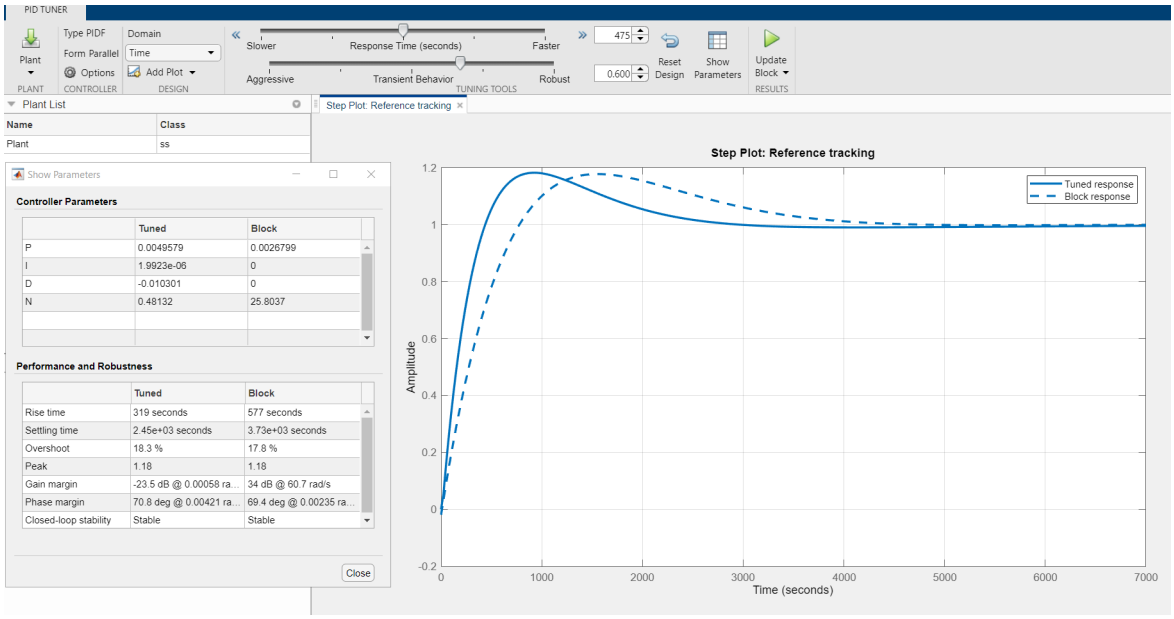

Figure A.2: PID Controller tuning using Simulink-PID Tuner

```
function [S1,S2,S3,S4,S5] = fcn( SOC1, SOC2, SOC3, SOC4, SOC5, SOC6)

%EVALUATE DIFFECRNCE BETWEEN THE CELLS
S12=abs(SOC1-SOC2);
S23=abs(SOC2-SOC3);
S34=abs(SOC3-SOC4);
S45=abs(SOC4-SOC5);
S56=abs(SOC5-SOC6);

%DIFFERENCE IN SoC BTW ADJACENT CELLS
SOCdiff = [S12, S23, S34, S45, S56];  % SoC difference array
dynamicMax = SOCdiff(1);  % Initialize dynamic maximum SoC difference with the first element
maxIndex = 1;  % Initialize index of dynamic maximum

for i = 2:length(SOCdiff)
    if SOCdiff(i) > dynamicMax
        dynamicMax = SOCdiff(i);  % Update dynamic maximum if a larger value is found
        maxIndex = i;  % Update index of dynamic maximum
    end
end
    if all(maxIndex == 1) && all(dynamicMax >= 0.0009)
        S1=1;
    elseif all(maxIndex == 2) && all(dynamicMax >= 0.0009)
        S2=1;
    elseif all(maxIndex == 3) && all(dynamicMax >= 0.0009)
        S3=1;
    elseif all(maxIndex == 4) && all(dynamicMax >= 0.0009)
        S4=1;
    elseif all(maxIndex == 5) && all(dynamicMax >= 0.0009)
        S5=1;
    end

end
```

Figure A.3: MATLAB function/algorithm for "Max-SoC difference approach"

DEPARTMENT OF SOME SUBJECT OR TECHNOLOGY
CHALMERS UNIVERSITY OF TECHNOLOGY
Gothenburg, Sweden
www.chalmers.se

CHALMERS
UNIVERSITY OF TECHNOLOGY